ARTICLES
https://doi.org/10.1038/s41588-018-0127-7

nature genetics

Genome-wide association meta-analysis highlights light-induced signaling as a driver for refractive error

Milly S. Tedja[1,2,80], Robert Wojciechowski[3,4,5,80], Pirro G. Hysi[6,80], Nicholas Eriksson[7,80], Nicholas A. Furlotte[7,80], Virginie J. M. Verhoeven[1,2,8,80], Adriana I. Iglesias[1,2,8], Magda A. Meester-Smoor[1,2], Stuart W. Tompson[9], Qiao Fan[10], Anthony P. Khawaja[11,12], Ching-Yu Cheng[10,13], René Höhn[14,15], Kenji Yamashiro[16], Adam Wenocur[17], Clare Grazal[17], Toomas Haller[18], Andres Metspalu[18], Juho Wedenoja[19,20], Jost B. Jonas[21,22], Ya Xing Wang[22], Jing Xie[23], Paul Mitchell[24], Paul J. Foster[12], Barbara E. K. Klein[9], Ronald Klein[9], Andrew D. Paterson[25], S. Mohsen Hosseini[25], Rupal L. Shah[26], Cathy Williams[27], Yik Ying Teo[28,29], Yih Chung Tham[13], Preeti Gupta[30], Wanting Zhao[10,31], Yuan Shi[31], Woei-Yuh Saw[32], E-Shyong Tai[29], Xue Ling Sim[29], Jennifer E. Huffman[33], Ozren Polašek[34], Caroline Hayward[33], Goran Bencic[35], Igor Rudan[36], James F. Wilson[33,36], CREAM[37], 23andMe Research Team[37], UK Biobank Eye and Vision Consortium[37], Peter K. Joshi[36], Akitaka Tsujikawa[16], Fumihiko Matsuda[38], Kristina N. Whisenhunt[9], Tanja Zeller[39], Peter J. van der Spek[40], Roxanna Haak[40], Hanne Meijers-Heijboer[41,42], Elisabeth M. van Leeuwen[1,2], Sudha K. Iyengar[43,44,45], Jonathan H. Lass[43,44], Albert Hofman[2,46,47], Fernando Rivadeneira[2,47,48], André G. Uitterlinden[2,47,48], Johannes R. Vingerling[1], Terho Lehtimäki[49,50], Olli T. Raitakari[51,52], Ginevra Biino[53], Maria Pina Concas[54], Tae-Hwi Schwantes-An[4,55], Robert P. Igo Jr[43], Gabriel Cuellar-Partida[56], Nicholas G. Martin[57], Jamie E. Craig[58], Puya Gharahkhani[56], Katie M. Williams[6], Abhishek Nag[59], Jugnoo S. Rahi[12,60,61], Phillippa M. Cumberland[60], Cécile Delcourt[62], Céline Bellenguez[63,64,65], Janina S. Ried[66], Arthur A. Bergen[41,67,68], Thomas Meitinger[69,70], Christian Gieger[66], Tien Yin Wong[71,72], Alex W. Hewitt[23,73,74], David A. Mackey[23,73,74], Claire L. Simpson[4,75], Norbert Pfeiffer[15], Olavi Pärssinen[76,77], Paul N. Baird[23], Veronique Vitart[33], Najaf Amin[2], Cornelia M. van Duijn[2], Joan E. Bailey-Wilson[4], Terri L. Young[9], Seang-Mei Saw[29,78], Dwight Stambolian[17], Stuart MacGregor[56], Jeremy A. Guggenheim[26,81], Joyce Y. Tung[7,81], Christopher J. Hammond[6,81] and Caroline C. W. Klaver[1,2,79,81*]

Refractive errors, including myopia, are the most frequent eye disorders worldwide and an increasingly common cause of blindness. This genome-wide association meta-analysis in 160,420 participants and replication in 95,505 participants increased the number of established independent signals from 37 to 161 and showed high genetic correlation between Europeans and Asians (>0.78). Expression experiments and comprehensive in silico analyses identified retinal cell physiology and light processing as prominent mechanisms, and also identified functional contributions to refractive-error development in all cell types of the neurosensory retina, retinal pigment epithelium, vascular endothelium and extracellular matrix. Newly identified genes implicate novel mechanisms such as rod-and-cone bipolar synaptic neurotransmission, anterior-segment morphology and angiogenesis. Thirty-one loci resided in or near regions transcribing small RNAs, thus suggesting a role for post-transcriptional regulation. Our results support the notion that refractive errors are caused by a light-dependent retina-to-sclera signaling cascade and delineate potential pathobiological molecular drivers.

Refractive errors are common optical aberrations determined by mismatches in the focusing power of the cornea, lens and axial length of the eye. Their distribution worldwide is rapidly shifting toward myopia, or nearsightedness. The myopia boom is particularly prominent in urban East Asia, where up to 95% of 20-year-olds in cities such as Seoul and Singapore have this

A full list of authors and affiliations appears at the end of the paper.

refractive error[1–4]. The prevalence of myopia is also rising throughout Western Europe and the United States, affecting ~50% of young adults in these regions[5,6]. Although refractive errors can be optically corrected, even at moderate values they carry substantial risk of ocular complications with high economic burden[7–9]. One in three individuals with high myopia (–6 diopters or worse) develop irreversible visual impairment or blindness, mostly as a result of myopic macular degeneration, retinal detachment or glaucoma[10,11]. At the other extreme, high hyperopia predisposes individuals to strabismus, amblyopia and angle-closure glaucoma[10,12].

Refractive errors result from a complex interplay of lifestyle and genetic factors. The most established lifestyle factors for myopia are high education, lack of outdoor exposure and excessive near work[3]. Recent research has identified many genetic variants for refractive errors, myopia and axial length[13–25]. Two large studies—the International Consortium for Refractive Error and Myopia (CREAM)[26] and the personal genomics company 23andMe, Inc.[17,27]—have provided the most comprehensive results[28].

Given that only 3.6% of the variance of the refractive-error trait was explained by the identified genetic variants[26], we presumed a high missing heritability. We therefore combined data from CREAM and 23andMe, and expanded the study sample to 160,420 individuals from a mixed-ancestry population with quantitative information on refraction for a genome-wide association study (GWAS) meta-analysis. Index variants were tested for replication in an independent cohort consisting of 95,505 individuals from the UK Biobank. We conducted systematic comparisons to assess differences in genetic inheritance and the distribution of risk variants between Europeans and Asians. Polygenic risk analyses were performed to evaluate the contributions of the identified variants to the risk of myopia and hyperopia. Finally, we integrated expression data and bioinformatics on the identified genes to gain insight into the possible mechanisms underlying the genetic associations.

Results

Susceptibility loci for refractive error. We performed a GWAS meta-analysis on adult untransformed spherical equivalent (SphE), using summary statistics from 37 studies from CREAM, and on age of diagnosis of myopia (AODM) from two cohorts from 23andMe[26,27] (Supplementary Fig. 1 and Supplementary Table 1a). The analyses were based on ~11 million genetic variants (SNPs, insertions and deletions) genotyped or imputed to the 1000 Genomes Project Phase I reference panel (version 3, March 2012 release[29]) that passed extensive quality control (Supplementary Figs. 2–4 and Supplementary Table 1b).

Meta-analyses were conducted in three stages: stage 1, CREAM (European dataset, CREAM-EUR, number of participants (n) = 44,192; Asian dataset, CREAM-ASN, n = 11,935); stage 2, 23andMe (n = 104,293; Methods); stage 3, joint meta-analysis of stages 1 and 2. Because CREAM and 23andMe applied different phenotype measures, we used signed Z scores as the mean per-allele effect size and assigned equal weights to CREAM and 23andMe. We identified 7,967 genome-wide-significant genetic variants clustering in 140 loci (Fig. 1a,b, Supplementary Figs. 5 and 6, Supplementary Tables 2–5 and Supplementary Data 1 and 2), replicating all 37 previously discovered loci and finding 104 novel loci. We applied genomic control at each stage and checked for population stratification by using linkage disequilibrium (LD)-score regression[30] (stage 1 and 2 inflation factors (GC) <1.1 and LD-score regression intercepts ($LDSC_{intercept}$) 0.892–1.023; Supplementary Table 6 and Supplementary Figs. 6 and 7). At stage 3, we observed genomic inflation ($\lambda GC = 1.129$; Supplementary Fig. 6), probably because of true polygenicity rather than population stratification or cryptic relatedness[31]. $LDSC_{intercept}$ remained undetermined, owing to mixed ancestry.

To detect the presence of multiple independent signals at the discovered loci, a stepwise conditional analysis was performed with GCTA-COJO[32] on summary statistics from all European cohorts (n = 148,485), with the Rotterdam Study I–III (RSI–III) used as a reference panel for LD structure ($n_{RSI-III}$ = 10,775). This analysis yielded 27 additional independent variants, thus resulting in a total of 167 loci (Supplementary Table 2).

We advanced these loci for replication in a GWAS of refractive error carried out by the UK Biobank Eye & Vision (UKEV) Consortium (n = 95,505)[33] (Methods). Six out of the 167 variants were not considered for replication analysis. One of these five variants (rs3138141, *RDH5*) was identified previously and therefore still considered a refractive-error risk variant[26,27]. The remaining 161 genetic variants were tested for replication. Among the candidate variants, 86% (138/161) replicated: 104 (65%) replicated surpassing genome-wide significance, and 34 replicated surpassing Bonferroni correction ($P < 3.0 \times 10^{-4}$; 21.1%); another 12 showed nominal evidence for replication ($0.05 < P < 3.0 \times 10^{-4}$; 7.5%); and only 11 (7%) did not replicate at all (Table 1 and Supplementary Table 2).

Because CREAM and 23andMe used different phenotypic outcomes, we evaluated the consistency of genotypic effects by comparing marker-wise additive genetic effect sizes (in diopters per risk-allele variant) for SphE from CREAM-EUR against those (in log(hazard ratio(HR)) per risk-allele variant) for AODM from 23andMe. All variants that were strongly associated with either outcome ($P < 0.001$) were concordant in direction of effect and had highly correlated effect sizes (Fig. 2a,b and Supplementary Fig. 8). For these variants, a 10% decrease in log(HR) for AODM, indicating an earlier age at myopia onset, was associated with a decrease of 0.15 diopters in SphE. A quantitative analysis of all common SNPs (minor allele frequency (MAF) >0.01; HapMap3) through LD-score regression yielded a genetic correlation of 0.93 (95% confidence interval (CI) 0.86–0.99; $P = 2.1 \times 10^{-159}$), thus confirming that the effect sizes for both phenotypic outcomes were closely related.

Gene annotation of susceptibility loci. We annotated all genetic variants with wANNOVAR by using the University of California Santa Cruz (UCSC) Known Gene database (see URLs)[34]. The 139 identified genetic loci were annotated to 208 genes and known transcribed RNA genes (Table 1, Supplementary Table 2 and Methods). The physical positions of the lead genetic variants relative to protein-coding genes are shown in Fig. 1c. 86% of the identified variants were either intragenic or less than 50 kb from the 5′ or 3′ end of the transcription start site. We found seven exonic variants (Supplementary Table 7), of which two had MAF ≤0.05: rs5442 (*GNB3*) and rs17400325 (*PDE11A*). The index SNP in the *GNB3* locus with MAF 0.05 in Europeans is a highly conserved missense variant (p.Gly272Ser) predicted to be damaging by PolyPhen-2 (ref. [35]) and SIFT[36]. *PDE11A* is presumed to play a role in tumorigenesis, brain function and inflammation[37]. The index SNP in the *PDE11A* locus with MAF 0.03 in Europeans is also a highly conserved missense variant (p.Tyr727Cys); this variant was predicted to be damaging by PolyPhen-2, SIFT[38] and align GVGD[39,40].The other exonic variants, rs1064583 (*COL10A1*), rs807037 (*KAZALD1*), rs1550094 (*PRSS56*), rs35337422 (*RD3L*) and rs6420484 (*TSPAN10*), were not predicted to be damaging.

The most significant variant (stage 3; rs12193446, $P = 4.21 \times 10^{-84}$) resides on chromosome 6 within a noncoding-RNA sequence, *BC035400*, in an intron of the *LAMA2* gene. This locus had been identified previously, but our current fine mapping redefined the most associated variant. The function and potential downstream target sites of *BC035400* are currently unknown. The previously most strongly associated variant, rs524952 on chromosome 15 near *GJD2*, was the second most significant variant ($P = 2.28 \times 10^{-65}$).

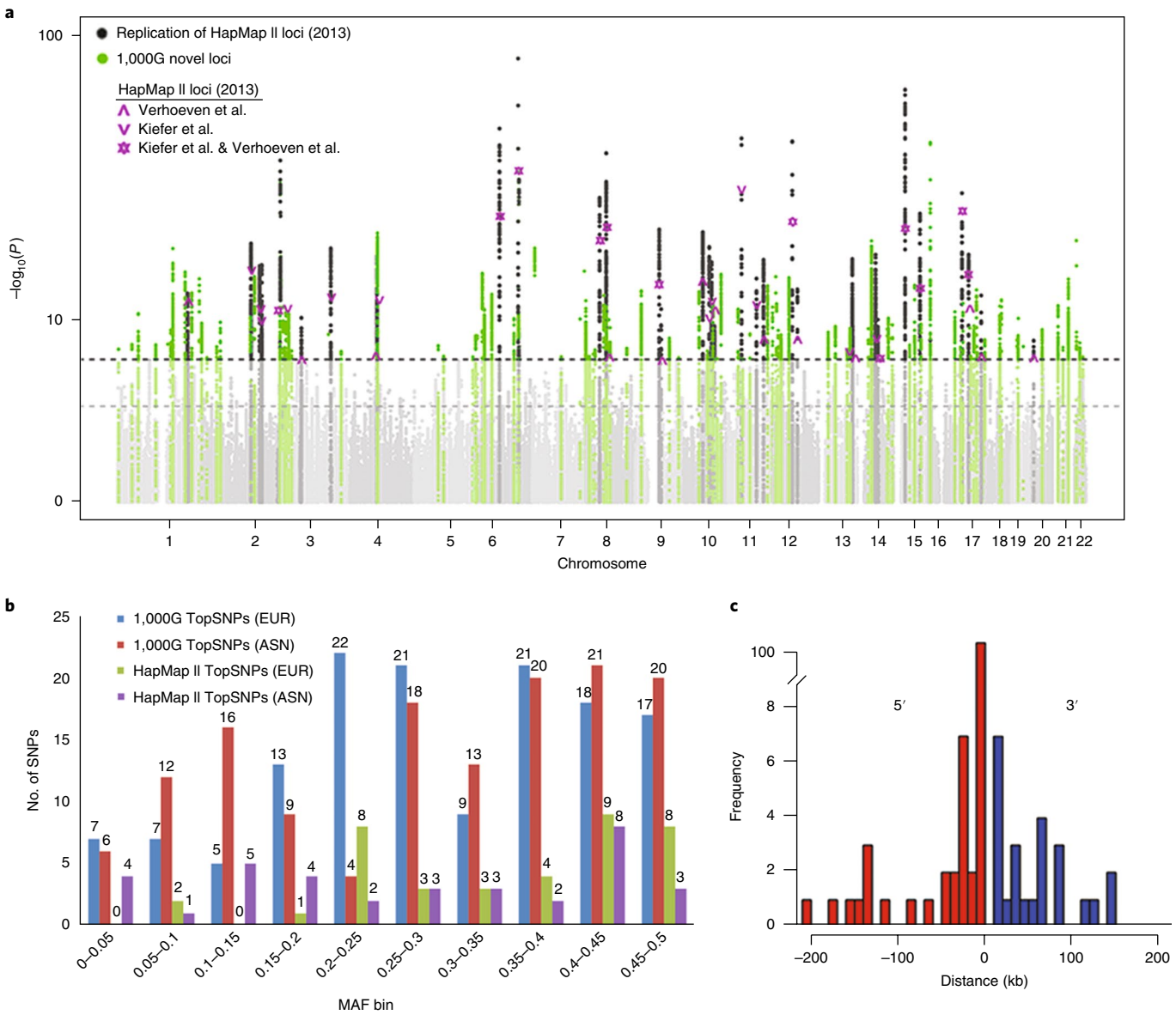

Fig. 1 | GWAS meta-analysis identifies 140 loci for refractive error (stage 3). a, Meta-analysis of genome-wide single-variant analyses for >10 million variants in 160,420 CREAM and 23andMe participants (stage 3). Shown is a Manhattan plot depicting *P* for association, highlighting newly identified ($P<5\times10^{-8}$; green) and known (dark gray) refractive-error loci previously found by using HapMap II imputations from Kiefer et al.[27] and Verhoeven et al.[26] (Table 1). The horizontal lines indicate suggestive significance ($P=1\times10^{-5}$) or genome-wide significance ($P=5\times10^{-8}$). 1000G, 1000 Genomes Project. **b**, MAFs of the 140 discovered index variants based on 1000G (blue, Europeans; red, Asians) to the MAFs of the previously found genetic variants based on HapMap II (green, Europeans; purple, Asians). An increase was observed in genetic variants found across all MAF bins, including the lower MAF bins. **c**, Annotation of the 167 loci to genes in wANNOVAR. Shown are the distances between index variants from the nearest gene and its gene on the 5′ and/or 3′ site. Most index variants (84%) were at a distance of less than 50 kb up- or downstream from the annotated gene.

Post-GWAS analyses. We performed two gene-based tests, fastBAT[41] and EUGENE[42], and applied a functional enrichment approach with fgwas[43] (Methods). With fastBAT, we identified 13 genes at $P<2.0\times10^{-6}$, one of which (*CHD7*) had been identified previously[26,27]. Using EUGENE, we found seven genes at $P<2.0\times10^{-6}$ after incorporation of blood expression quantitative trail loci (eQTLs). With fgwas, we identified six loci, which were annotated to nine genes, at a posterior probability >0.9. Two genes (*HMGN4* and *TLX1*) showed significant associations in two or more approaches. Together, these post-GWAS approaches resulted in a total of 22 additional candidate loci for refractive error, annotated to 25 genes (Supplementary Table 8). These results increase the overall number of significant genetic associations to 161 candidate loci.

Polygenic risk scores. We calculated polygenic risk scores (PGRS)[44] per individual at various *P* thresholds (Methods) for RSI–III ($n=10{,}792$) after recalculating *P* and *Z* scores of variants from stage 3 excluding RSI–III. The highest fraction of phenotypic variance (7.8%) was explained with 7,307 variants at a *P*-value threshold of 0.005 (Supplementary Table 9). A PGRS based on these variants distinguished between individuals with hyperopia and myopia at the lower and higher deciles (Fig. 3); those in the highest decile had a 40-fold-greater risk of myopia. When the PGRS was stratified for the median age (<63 or >63 years), we found a significant difference in the variance explained (<63 years, 8.9%; >63 years, 7.4%; $P=0.0038$). The variance explained by PGRS was not significantly different between males and females

Table 1 | Results of the meta-analysis of CREAM and 23andMe for the previously identified loci and a subset of the newly identified loci, and replication in UK Biobank

Replication of the HapMap II index variants for refractive error per locus in the stage 3 meta-analysis														
SNP	**Chromosome**	**Position**	**Nearest loci and gene(s)**	**Effect allele**	**Other allele**	**EAF EUR**	**EAF ASN**	***Z* score**	**Direction**	***P* value**	**Het *I*sq**	**Het *P* value**	**Sample size (*n*)**	***P*-value replication**
rs12193446	6	129820038	*BC035400, LAMA2*	A	G	0.906	NA	-19.43	- -	4.21×10^{-84}	16.8	5.72×10^{-15}	150,269	4.60×10^{-106}
rs524952	15	35005886	*GOLGA8B, GJD2*	A	T	0.475	0.507	-17.08	- -	2.28×10^{-65}	67.2	0.015	160,150	1.60×10^{-103}
rs7744813	6	73643289	*KCNQ5*	A	C	0.591	0.602	-14.56	- -	5.43×10^{-48}	35	0.001	160,091	1.00×10^{-75}
rs11602008	11	40149305	*LRRC4C*	A	T	0.822	0.749	13.98	+ +	2.12×10^{-44}	22.5	1.56×10^{-10}	157,505	2.90×10^{-47}
rs3138141	12	56115778	*BLOC1S1-RDH5, RDH5*	A	C	0.214	0.147	13.8	+ +	2.46×10^{-43}	3.2	5.05×10^{-7}	157,531	2.30×10^{-56}
rs10500355	16	7459347	*RBFOX1*	A	T	0.354	0.133	-13.73	- -	6.49×10^{-43}	9.1	2.93×10^{-7}	160,139	2.50×10^{-48}
rs72621438	8	60178580	*SNORA51, CA8*	C	G	0.642	0.609	-13.14	--	2.03×10^{-39}	38.4	0.006	160,128	1.80×10^{-49}
rs1550094	2	233385396	*CHRNG, PRSS56*	A	G	0.701	0.705	12.74	+ +	3.64×10^{-37}	26.3	0.003	159,422	4.10×10^{-59}
rs2908972	17	11407259	*SHISA6*	A	T	0.415	0.484	-11.13	- -	9.46×10^{-29}	23	0.254	160,123	6.10×10^{-29}
rs7829127	8	40726394	*ZMAT4*	A	G	0.792	0.897	-10.91	- -	1.02×10^{-27}	15.9	2.77×10^{-4}	160,132	3.10×10^{-22}
rs6495367	15	79375347	*RASGRF1*	A	G	0.408	0.399	-10.2	- -	1.95×10^{-24}	0	0.667	160,144	7.20×10^{-37}
rs11145465	9	71766593	*TJP2*	A	C	0.212	NA	-9.55	- -	1.35×10^{-21}	46.3	0.1722	153,174	1.00×10^{-10}
rs1649068	10	60304864	*BICC1*	A	C	0.475	0.504	-9.44	- -	3.77×10^{-21}	0	0.712	160,144	7.50×10^{-11}
rs7692381	4	81903049	*CFAP299, BMP3*	A	G	0.763	0.63	9.4	+ +	5.55×10^{-21}	0	0.013	160,134	7.50×10^{-13}
rs56075542	2	146882415	*BC040861, PABPC1P2*	T	G	0.552	0.472	-8.99	- -	2.39×10^{-19}	13.9	0.001	159,478	1.30×10^{-18}
rs7895108	10	79061458	*KCNMA1*	T	G	0.351	0.118	-8.87	- -	7.56×10^{-19}	32.8	0.021	160,140	1.10×10^{-27}
rs7624084	3	141093285	*ZBTB38*	T	C	0.568	0.633	-8.81	- -	1.24×10^{-18}	18.5	0.018	160,151	6.50×10^{-17}
rs62070229	17	31227593	*MYO1D, TMEM98*	A	G	0.807	0.874	8.58	+ +	9.64×10^{-18}	0	0.416	156,570	1.30×10^{-18}
rs2855530	14	54421917	*BMP4*	C	G	0.507	0.474	-8.58	- -	9.87×10^{-18}	41.7	0.19	160,092	4.80×10^{-22}
rs7662551	4	80537638	*LOC100506035, PCAT4*	A	G	0.723	0.558	8.53	+ +	1.47×10^{-17}	19.4	0.265	160,147	6.00×10^{-12}
rs9517964	13	100717833	*ZIC2, PCCA*	T	C	0.589	0.786	8.42	+ +	3.68×10^{-17}	0	0.02	160,121	3.40×10^{-20}
rs1954761	11	105596885	*GRIA4*	T	C	0.371	0.377	-8.4	- -	4.57×10^{-17}	0	0.911	160,122	1.20×10^{-16}
rs745480	10	85986554	*LRIT2, LRIT1*	C	G	0.511	0.418	8.31	+ +	9.26×10^{-17}	67.3	0.081	159,504	8.20×10^{-18}
rs2573081	2	178828507	*PDE11A*	C	G	0.524	0.538	8.21	+ +	2.18×10^{-16}	47.6	0.167	160,126	1.60×10^{-29}
rs17428076	2	172851936	*HAT1, METAP1D*	C	G	0.768	0.854	-8.18	- -	2.77×10^{-16}	0	0.003	160,151	7.50×10^{-8}
rs2155413	11	84634790	*DLG2*	A	C	0.482	0.655	-7.76	- -	8.85×10^{-15}	0	2.99×10^{-4}	159,504	1.10×10^{-17}
rs11178469	12	71275137	*PTPRR*	T	C	0.752	0.638	-7.4	- -	1.33×10^{-13}	0	0.6989	160,139	2.60×10^{-04}
rs1858001	1	207488004	*C4BPA, CD55*	C	G	0.676	0.415	7.28	+ +	3.45×10^{-13}	59.6	0.02	160,149	6.70×10^{-20}
rs4793501	17	68718734	*KCNJ2, BC039327*	T	C	0.575	0.444	-7.21	- -	5.53×10^{-13}	0	0.592	160,150	3.70×10^{-12}
rs7042950	9	77149837	*RORB*	A	G	0.732	0.392	6.8	+ +	1.07×10^{-11}	0	0.912	160,153	2.90×10^{-18}

Continued

Table 1 | Results of the meta-analysis of CREAM and 23andMe for the previously identified loci and a subset of the newly identified loci, and replication in UK Biobank (Continued)

Replication of the HapMap II index variants for refractive error per locus in the stage 3 meta-analysis														
SNP	**Chromosome**	**Position**	**Nearest loci and gene(s)**	**Effect allele**	**Other allele**	**EAF EUR**	**EAF ASN**	***Z* score**	**Direction**	***P* value**	**Het *I*sq**	**Het *P* value**	**Sample size (*n*)**	***P*-value replication**
rs4687586	3	53837971	*CACNA1D*	C	G	0.691	NA	-6.55	- -	5.86×10^{-11}	0	0.605	150,217	1.60×10^{-8}
rs2753462	14	60850703	*JB175233, C14orf39*	C	G	0.296	0.568	-6.49	- -	8.37×10^{-11}	73.9	0.05	157,352	2.00×10^{-15}
rs837323	13	101175664	*PCCA*	T	C	0.512	0.762	6.32	+ +	2.65×10^{-10}	35.6	0.213	160,142	5.30×10^{-16}
rs17382981	10	94953258	*CYP26A1, MYOF*	T	C	0.417	0.19	-6.31	- -	2.72×10^{-10}	67.9	0.077	155,332	4.10×10^{-7}
rs79266634	16	7309047	*RBFOX1*	C	G	0.093	0.115	-5.93	- -	3.00×10^{-9}	0	0.561	156,268	1.50×10^{-8}
rs235770	20	6761765	*BMP2*	T	C	0.372	0.388	-5.93	- -	3.11×10^{-9}	0	0.547	157,521	4.80×10^{-11}
rs36024104	14	42294993	*LRFN5*	A	G	0.823	NA	9.09	++	9.86×10^{-20}	15.9	0.01414	152,585	2.20×10^{-12}
rs1556867	1	164213686	*5S_rRNA, PBX1*	T	C	0.264	0.494	-8.81	- -	1.29×10^{-18}	71.1	0.06266	160,155	4.20×10^{-17}
rs2225986	1	200311910	*LINC00862*	A	T	0.381	0.169	-7.96	- -	1.68×10^{-15}	40.2	0.196	160,152	7.50×10^{-17}
rs1207782	6	22059967	*LINC00340*	T	C	0.577	0.265	-7.92	- -	2.47×10^{-15}	0	0.8946	160,149	4.90×10^{-13}
rs72826094	10	114801488	*TCF7L2*	A	T	0.799	0.838	7.88	++	3.20×10^{-15}	64.5	0.09323	156,825	4.90×10^{-2}
rs297593	2	157363743	*GPD2*	T	C	0.286	0.257	-7.82	- -	5.45×10^{-15}	0	0.5285	159,461	7.80×10^{-11}
rs5442	12	6954864	*GNB3*	A	G	0.068	NA	-7.82	- -	5.48×10^{-15}	8.8	0.03693	146,217	1.20×10^{-33}
rs10880855	12	46144855	*ARID2*	T	C	0.507	0.464	-7.78	- -	7.35×10^{-15}	0	0.9683	160,144	4.80×10^{-8}
rs2150458	21	47377296	*PCBP3, COL6A1*	A	G	0.455	0.641	7.74	++	1.04×10^{-14}	55.7	0.1329	160,151	1.80×10^{-13}
rs12898755	15	63574641	*APH1B*	A	G	0.245	0.456	7.53	++	4.98×10^{-14}	7.9	0.2974	159,506	1.40×10^{-16}
rs7122817	11	117657679	*DSCAML1*	A	G	0.507	0.662	7.51	++	5.73×10^{-14}	73.8	0.05077	160,147	1.10×10^{-10}
rs10511652	9	18362865	*SH3GL2, ADAMTSL1*	A	G	0.416	0.445	7.36	++	1.91×10^{-13}	44.8	0.1782	160,149	3.50×10^{-18}
rs11101263	10	49414181	*FRMPD2*	T	C	0.258	0.105	-7.33	- -	2.33×10^{-13}	0	0.3477	160,155	2.20×10^{-13}
rs11118367	1	219790221	*LYPLAL1*	T	C	0.482	0.630	-7.29	- -	3.16×10^{-13}	0	0.8576	160,141	1.20×10^{-13}
rs9395623	6	50757699	*TFAP2D, TFAP2B*	A	T	0.315	0.381	7.25	++	4.16×10^{-13}	0	0.9579	160,151	2.20×10^{-10}
rs284816	8	53362145	*ST18, FAM150A*	A	G	0.163	0.198	-7.21	- -	5.52×10^{-13}	0	0.9242	160,140	1.60×10^{-8}
rs12965607	18	47391025	*MYO5B*	T	G	0.857	0.923	7.07	++	1.52×10^{-12}	20.8	0.01674	157,604	8.10×10^{-16}
rs7747	4	80827062	*ANTXR2*	T	C	0.202	0.093	7.03	++	2.05×10^{-12}	5.4	0.01267	150,327	7.70×10^{-16}
rs12451582	17	54734643	*NOG, C17orf67*	A	G	0.369	0.308	7.02	++	2.22×10^{-12}	0	0.5925	160,155	8.80×10^{-18}
rs80253120	17	14138507	*CDRT15*	T	C	0.626	0.723	6.97	++	3.25×10^{-12}	58.6	0.12	156,054	7.20×10^{-11}
rs7968679	12	9313304	*PZP*	A	G	0.700	0.894	6.95	++	3.65×10^{-12}	0	0.01951	160,076	4.20×10^{-10}
rs11202736	10	90142203	*RNLS*	A	T	0.717	0.762	-6.92	- -	4.53×10^{-12}	0	0.4007	160,150	9.40×10^{-7}
rs72655575	8	60556509	*SNORA51, CA8*	A	C	0.201	0.124	6.87	++	6.54×10^{-12}	0	0.8811	156,566	7.10×10^{-7}
rs1790165	11	131928971	*NTM*	A	C	0.411	0.283	6.85	++	7.17×10^{-12}	0	0.003708	160,131	1.80×10^{-10}
rs511217	11	30029948	*METTL15, KCNA4*	A	T	0.738	0.729	-6.79	- -	1.10×10^{-11}	0	0.3626	160,143	1.40×10^{-17}

We identified 140 loci for refractive error with genome-wide significance ($P<5\times10^{-8}$) on the basis of the meta-analyses of the genome-wide single-variant linear regressions performed in 160,420 participants of mixed ancestries (CREAM-ASN, CREAM-EUR and 23andMe). Shown are the replication of the previously found loci from HapMap II and a subset of the new loci with the smallest *P* values. For each locus, represented by an index variant (the variant with the smallest *P* value in that locus), effect allele, other allele, effect-allele frequencies per ancestry (EAF ASN and EAF EUR), effect size (*Z* score), direction of the effect (direction), the *P* value, heterogeneity *I* square (Het *I*sq), heterogeneity *P* value (Het *P* value), sample size (*n*) and *P* value of the replication in UK Biobank are shown (full table in Supplementary Table 2). ASN, Asian; EUR, European; GWS, genome wide significant; NA, not applicable.

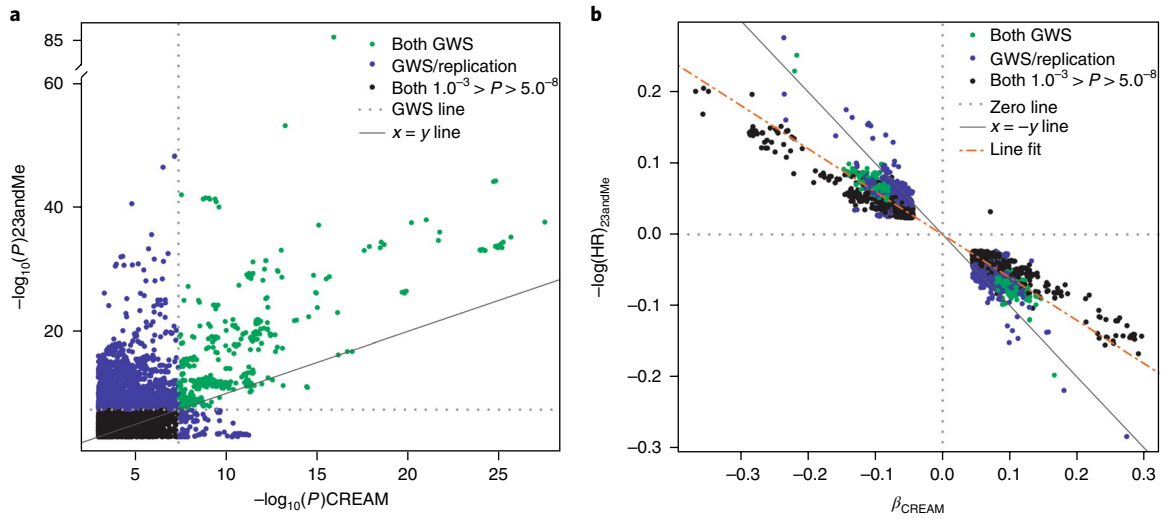

Fig. 2 | Correlation of statistical significance and effect size of SNPs on the basis of SphE in diopters and AODM in years. a, *P* comparison of all genetic variants with $P < 1.0 \times 10^{-3}$ ($n = 7{,}249$) between CREAM meta-analysis (stage 1) and 23andMe (stage 2) meta-analysis. Shown is the overlap (green) and the difference (purple) in *P* signals per cohort for genetic variants. Purple genetic variants are only genome wide significant (GWS) in either CREAM or 23andMe. Black, genetic variants with *P* between 5.0×10^{-8} and 1.0×10^{-3} in both CREAM and 23andMe. **b**, Comparison of effects (SphE and logHR of AODM in years; $P < 1.0 \times 10^{-3}$; $n = 7{,}249$) between CREAM and 23andMe, with color code as in **a**. The effects were concordant in their direction of effect on refractive error. We performed a simple linear regression between the effects of CREAM and 23andMe; the regression slope was −0.15 diopters per logHR of AODM in years.

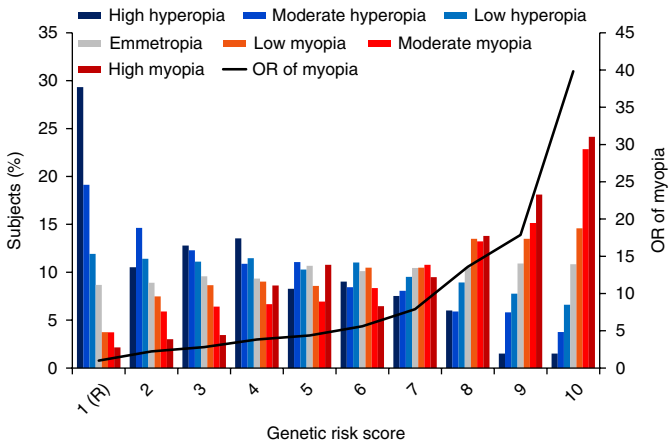

Fig. 3 | Risk of refractive error per decile of polygenic risk score (Rotterdam Study I–III, $n = 10{,}792$). Distribution of refractive error in subjects from RSI–III ($n = 10{,}792$) as a function of the optimal polygenic risk score (including 7,303 variants at $P \leq 0.005$ explaining 7.8% of the variance of SphE; Supplementary Table 9). The mean odds ratio (OR) of myopia (black line) was calculated per polygenic-risk-score category by using the lowest category as a reference. High myopia, SphE ≤−6 diopters; moderate myopia, SphE >−6 diopters and ≤−3 diopters; low myopia, SphE >−3 diopters and <-1.5 diopters; emmetropia, SphE ≥−1.5 diopters and ≤1.5 diopters; low hyperopia, SphE >1.5 diopters and <3 diopters; moderate hyperopia, SphE ≥3 diopters and 6 diopters; high hyperopia, SphE ≥6 diopters. (R), reference group.

(8.3 vs. 7.5%, respectively; $P = 0.13$). The predictive value (area under the receiver operating characteristic curve) of the PGRS for myopia vs. hyperopia, adjusted for age and sex, was 0.77 (95% CI = 0.75–0.79), a value 10% higher than previous estimations[45].

Transancestral comparison of genotypic effects. To explore potential ancestry differences in the identified refractive-error loci, we calculated the heritability explained by common genetic variants (SNP-h^2) for Europeans and Asians, by using LD-score regression[46]. The SNP-h^2 was 0.214 (95% CI 0.185–0.243) and 0.172 (95% CI 0.154–0.190) in the European samples (CREAM-EUR and 23andMe, respectively), but was only 0.053 (95% CI −0.025–0.131) in the Asian sample (CREAM-EAS). Next, we estimated the genetic correlation between Europeans and Asians by comparing variant effect sizes for common variants in Popcorn[47] (Methods). Two genetic correlation metrics were calculated: (i) a genetic-effect correlation (ρge) that quantifies the correlation in SNP effect sizes between Europeans and Asians without taking into account ancestry-related differences in allele frequency and (ii) a genetic-impact correlation (ρgi) that estimated the correlation in variance-normalized SNP effect sizes between the two ancestry groups (Table 2). Estimates of ρge were high between Europeans and Asians, but were significantly different from 1 (0.79 and 0.80, respectively, at $P < 1.9 \times 10^{-6}$; Table 2), thus indicating a clear genetic overlap but a difference in per-allele effect size. Estimates of ρgi were similarly high (>0.8) but were not significantly different from 1 for the correlation between CREAM-EUR and CREAM-ASN ($P = 0.065$), thus indicating that the genetic impact of these alleles may still be similar.

In silico pathway analysis. We used an array of bioinformatics tools to investigate potential functions and pathways of the associated genes. We first used DEPICT[48] to perform a gene set enrichment analysis, a tissue-type enrichment analysis and a gene prioritization analysis, on all variants with $P < 1.00 \times 10^{-5}$ from stage 3. The gene set enrichment analysis resulted in 66 reconstituted gene sets, of which 55 (83%) were eye related. To decrease redundancy among pathways, we clustered the significant pathways into 13 meta-gene sets (false discovery rate (FDR) <5% and $P < 0.05$) (Supplementary Note, Fig. 4 and Supplementary Table 10). The most significant gene set was 'abnormal photoreceptor inner segment morphology' (Mammalian Phenotype Ontology (MP) 0003730; $P = 1.79 \times 10^{-7}$). The eye-related meta-gene sets consisted of 'thin retinal outer nuclear layer' (MP 0008515; 27 (55%) gene sets), 'detection of light stimulus' (Gene Ontology (GO) 0009583; 13 (24%) gene sets), 'nonmotile primary cilium' (GO 0031513; 4 (6%) gene sets) and 'abnormal

Table 2 | Genetic correlation for refractive error between Europeans and East Asians

Sample 1	Sample 2	Genetic effect correlation (ρge)[a]	Standard error ρge	*P* value ρge	Genetic impact correlation (ρgi)[a]	Standard error ρgi	*P* value ρgi
EUR CREAM	EAS CREAM	0.804	0.041	1.83×10^{-6}	0.888	0.061	0.065
EUR 23andMe	EAS CREAM	0.788	0.041	2.48×10^{-7}	0.865	0.054	0.014

Abbreviations: EUR, European; EAS, East Asian. [a]*P* value relates to a test of the null hypothesis that ρge = 1 or ρgi = 1. We calculated the genetic correlation of effect (ρge) and impact (ρgi) by using Popcorn to compare the genetic associations between Europeans (CREAM-EUR, *n* = 44,192; 23andMe, *n* = 104,292) and East Asians (CREAM-ASN, *n* = 9,826). Reference panels for Popcorn were constructed with genotype data for 503 EUR and 504 EAS individuals sequenced as part of the 1000 Genomes Project. SNPs used had a MAF of at least 5% in both populations, thus resulting in a final set of 3,625,602 SNPs for the 23andMe GWAS sample and 3,642,928 SNPs for the CREAM-EUR sample. These findings support a largely common genetic predisposition to refractive error and myopia in Europeans and Asians, although ancestry-specific risk alleles may exist.

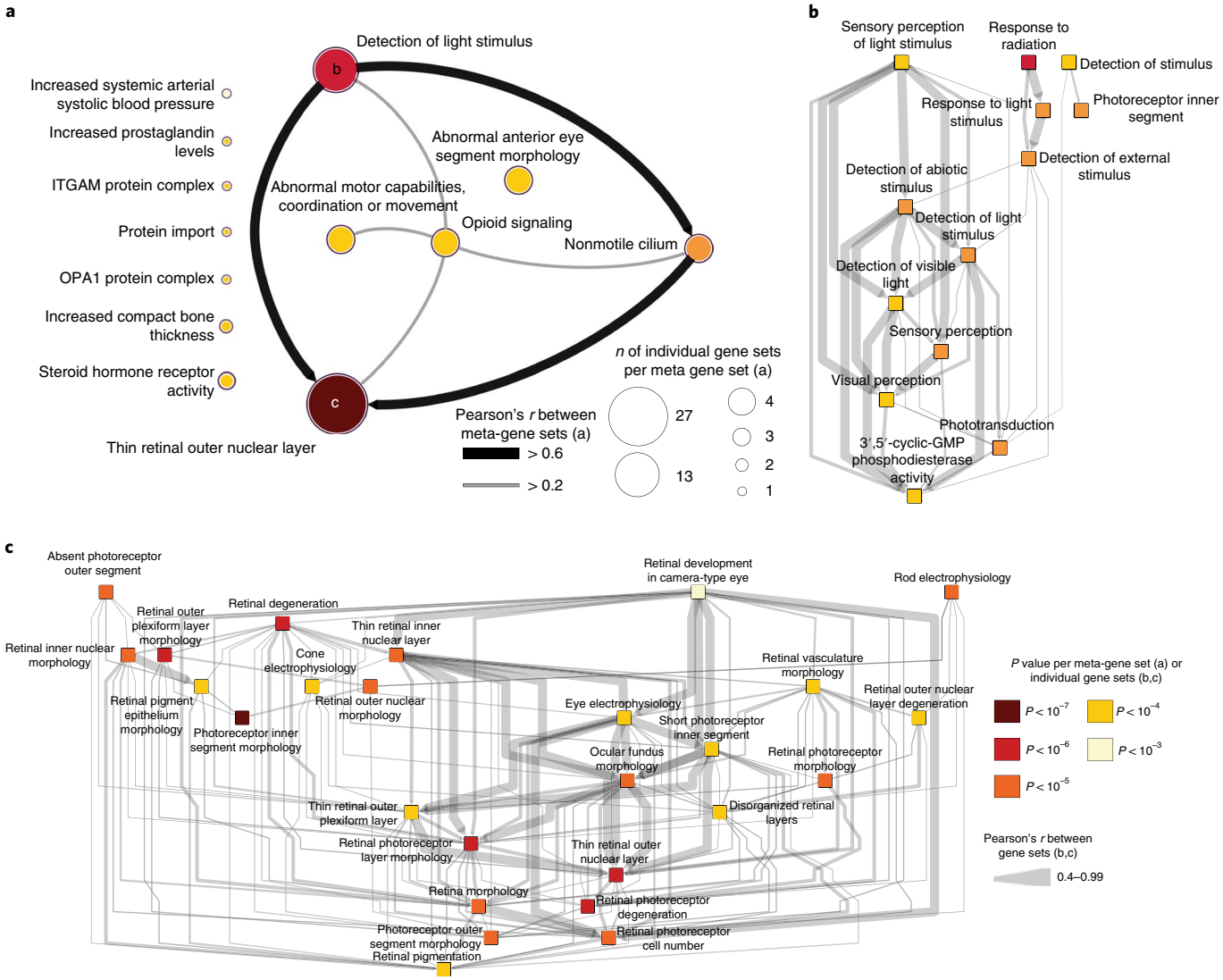

Fig. 4 | Visualization of the DEPICT gene set enrichment analysis based on loci associated with refractive error and the correlation between the (meta) gene sets. a, The 66 significantly enriched reconstituted gene sets clustered into 13 meta-gene sets on the basis of the gene set enrichment analysis of DEPICT (pairwise Pearson correlations; $P < 0.05$). All genetic variants with $P < 1\times10^{-5}$ in the GWAS meta-analysis of stage 3 ($n = 21{,}073$) and an FDR < 0.05 were considered. **b**, Visualization of the interconnectivity among gene sets ($n = 13$; pairwise Pearson correlations; $P < 0.05$) of the meta-gene set 'detection of light stimulus' (GO 0009583). **c**, Visualization of the interconnectivity between gene sets ($n = 27$; pairwise Pearson correlations; $P < 0.05$) of the largest meta-gene set 'thin retinal outer nuclear layer' (MP 0008515). In all panels, (meta)gene sets are represented by nodes colored according to statistical significance, and similarities among them are indicated by edges scaled according to their correlation; Pearson's $r \geq 0.2$ are shown in a, and Pearson's $r \geq 0.4$ are shown in **b**,**c**.

anterior-eye-segment morphology' (MP 0005193; 4 (6%) gene sets). The first three meta-gene sets had a Pearson's correlation >0.6. Interestingly, *RGR*, *RP1L1*, *RORB* and *GNB3* were present in all of these meta-gene sets. The retina was the most significant tissue of expression according to the tissue-type enrichment analysis ($P = 1.11\times10^{-4}$, FDR < 0.01). From the gene prioritization according

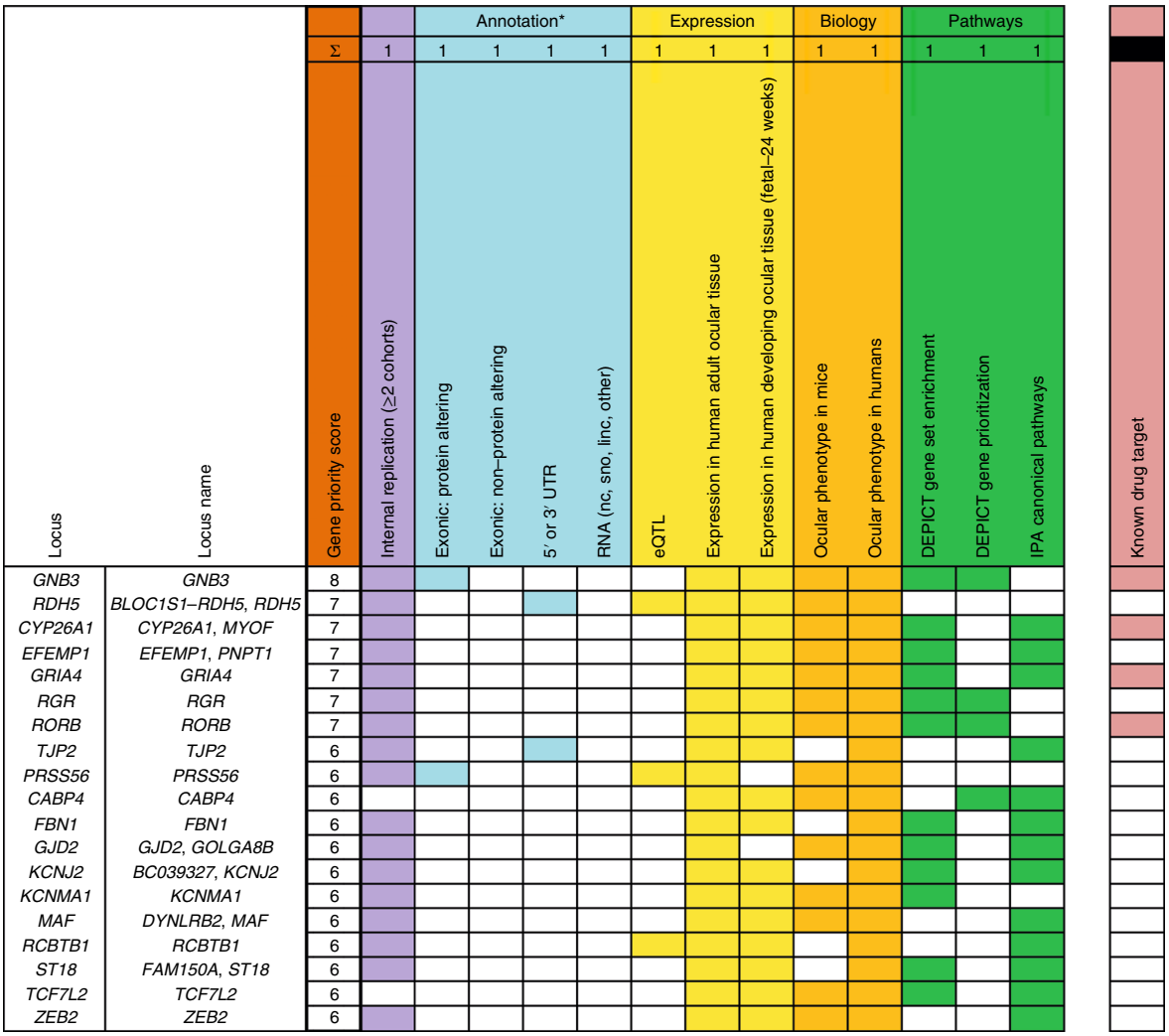

Fig. 5 | Genes ranked according to biological and statistical evidence. Genes ranked (orange) according to ten equal categories that can be grouped into the following: internal replication of genetic variant in two or more cohorts (purple; CREAM-EUR, CREAM-ASN and/or 23andMe); annotation (light blue; genetic variant bearing an exonic protein-altering variant or non-protein-altering variant, genetic variant residing in a 5′ or 3′ UTR of a gene or transcribing an RNA structure); expression (yellow; eQTL, expression in adult human ocular tissue, expression in developing ocular tissue); biology (dark yellow; ocular phenotype in mice, ocular phenotype in humans); pathways (green; DEPICT gene set enrichment, DEPICT gene-prioritization analysis and IPA canonical pathway analysis). We assessed genes bearing drug targets (salmon red) but did not assign a scoring point to that category. Asterisk indicates that only one point could be assigned for 'annotation', even though it has four columns (i.e., a genetic variant is located in only one of these four categories).

to DEPICT, seven genes were highlighted as the most likely causal genes at $P<7.62\times10^{-6}$ and FDR<0.05: *ANO2*, *RP1L1*, *GNB3*, *EDN2*, *RORB* and *CABP4*.

Next, we performed a canonical pathway analysis on all genes annotated to the variants of stage 3, by using Ingenuity Pathway Analysis (IPA; see URLs). All genes were run against the IPA database incorporating functional biological evidence on genomic and proteomic expression according to regulation or binding studies. IPA identified 'glutamate receptor signaling' with the central player NF-κB as the most significant pathway after correction for multiple testing (ratio of the number of molecules, 8.8%; Fisher's exact $P=1.56\times10^{-4}$; Supplementary Fig. 9).

From disease-associated loci to biological mechanisms. We adapted the scoring scheme designed by Fritsche et al.[49] to highlight genes with biologically plausible roles in eye growth. We used ten equally rated categories (Methods, Fig. 5, Supplementary Table 11 and Supplementary Note). We found that 109 index variants replicated in two or more individual cohorts; there was evidence for seven genetic variants with eQTL effects in multiple tissue types; nine exonic variants, seven of which predicted protein alterations (Supplementary Table 7); 31 RNA genes, five of which were located in the 3′ or 5′ untranslated region (UTR) (Supplementary Table 12 and Supplementary Fig. 10); 84 genes resulting in an ocular phenotype in humans (Supplementary Table 13) and 36 in mice (Supplementary Table 14); 172/212 (81%) genes expressed in human ocular tissue (Supplementary Note and Supplementary Table 15); 41 genes identified by DEPICT at $P<5.4\times10^{-4}$ and FDR<0.05; and 45 genes that contributed to the most significant canonical IPA pathways. Notably, 48 of the associated genes encode known drug targets (Supplementary Table 16).

The gene with the highest biological-plausibility score (score = 8) was *GNB3*, a highly conserved gene encoding a G-nucleotide-binding protein expressed in rod and cone photoreceptors and ON bipolar cells[50]. *GNB3* participates in signal transduction through G-protein-coupled receptors and enhances the temporal accuracy

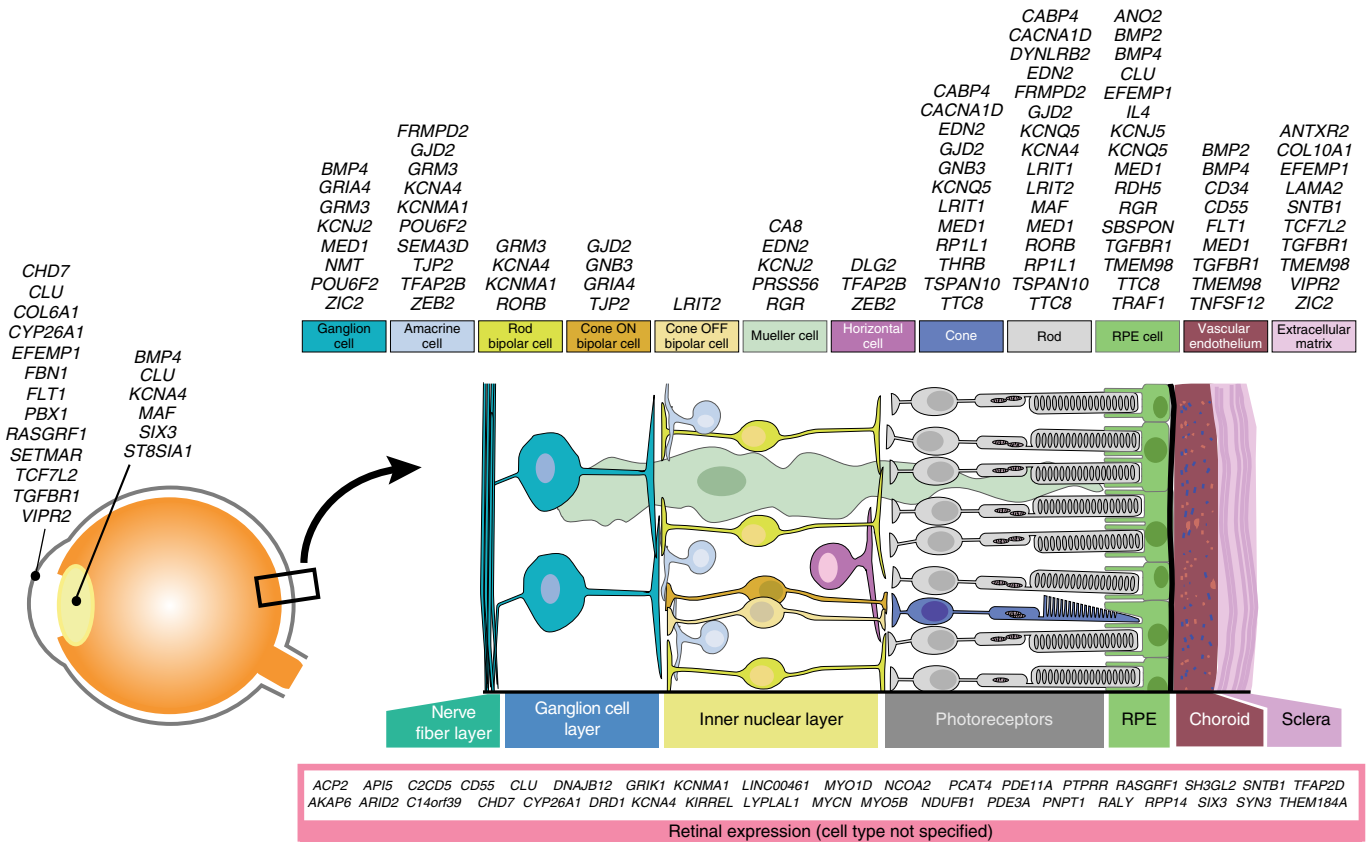

Fig. 6 | Schematic representation of the human eye, retinal cell types and functional sites of associated genes. We assessed gene expression sites and/or functional target cells in the eye for all genes by using our expression data, data from the literature and data present in the public domain. The genes appeared to be distributed across all cell types in the neurosensory retina, in the RPE, vascular endothelium and extracellular matrix; i.e., the route of the myopic retina-to-sclera signaling cascade.

of phototransduction and ON-center signaling in the retina[50]. As described above, the index SNP contains a missense variant associated with refractive errors. Nonsynonymous mutations within *GNB3* are known to cause syndromic congenital stationary night blindness[51] in humans; progressive retinopathy and globe enlargement in chickens[50]; and abnormal development of the photoreceptor-bipolar synapse in knockout mice[52,53].

Other highly ranked (score = 7) genes included *CYP26A1*, *GRIA4*, *RDH5*, *RORB* and *RGR*, all previously associated with refractive error, and one newly identified gene, *EFEMP1*. *EFEMP1* encodes a member of the fibulin family of extracellular-matrix glycoproteins and is found panocularly, including in the inner nuclear layer and Bruch's membrane. Mutations in this gene lead to specific macular dystrophies[54], whereas variants have also been shown to cosegregate with primary open-angle glaucoma[55] and to be associated with optic disc cup area[56].

Several other genes were noteworthy for their function. *CABP4*, which encodes a calcium-binding protein expressed in cone and rod photoreceptor cells, mediates Ca^{2+} influx and glutamate release in the photoreceptor bipolar synapse[57]. Mutations in this gene have been described in congenital cone-rod synaptic disorder[58], a retinal dystrophy associated with nystagmus, photophobia and high hyperopia. *KCNMA1* encodes pore-forming alpha subunits of Ca^{2+}-activated K^+ channels. These channels regulate synaptic transmission exclusively in the rod pathway[59]. *ANO2* encodes a Ca^{2+}-activated Cl^- channel recently reported to regulate retinal pigment epithelium (RPE) cell volume in a light-dependent manner[60]. *EDN2* encodes a potent vasoconstrictor that binds to two G-protein-coupled receptors encoded by *EDNRA*, which resides on bipolar dendrites, and the protein product of *EDNRB*, which is present on Mueller and horizontal cells. Both receptors are also present on choroidal vessels[61], thus implying that the choroid as well as retinal cells are target sites of this gene. *RP1L1* is expressed in cone and rod photoreceptors, where it is involved in the maintenance of microtubules in the connecting cilium[62]. Mutations in this gene cause dominant macular dystrophy and retinitis pigmentosa[63]. We replicated two genes involved in myopia in family studies: (i) *FBN1*, which bears mutations causing Marfan (MIM 154700) and Weil Marchesani (MIM 608328) syndromes, and (ii) *PTPRR*, one of the candidates in the *MYP3* locus, which was identified on the basis of linkage in families with high myopia[64].

The location of rs7449443 ($P = 3.58 \times 10^{-8}$) is notable because it resides between *DRD1* and *LINC01951*. *DRD1* encodes dopamine receptor 1 and is known to modulate dopamine receptor 2–mediated events[65,66]. The dopamine pathway has been implicated in myopia pathogenesis in many studies[65,67]. SNPs in and near other genes involved in the dopamine pathway (dopamine receptor binding, synthesis, degradation and transport)[68–70] did not show genome-wide-significant associations (Supplementary Note, Supplementary Table 17 and Supplementary Fig. 11).

There were 31 genetic variants in or near DNA structures transcribing RNA genes (noncoding RNA, long intergenic noncoding RNAs, tRNAs, small nucleolar RNAs and ribosomal RNAs). Notably, five were in the transcription region, and 13 were in the vicinity (>0 kb and ≤50 kb) of the start or end of the transcription region. They received low scores because many have no reported function or disease association to date (Fig. 5, Supplementary Fig. 10

and Supplementary Table 12). Our ranking of genes according to functional information existing in the public domain does not necessarily represent the true order of importance for refractive-error pathogenesis. The observation that genes with strong statistical association were distributed over all scores supports this concept. Nevertheless, this list may aid in selection of genes for subsequent functional studies.

Finally, integration of all our findings together with literature allowed us to annotate a large number of genes to ocular cell types (Fig. 6). All cell types of the retina contained refractive-error genes, as well as RPE, vascular endothelium and extracellular matrix.

Genetic pleiotropy. We performed a GWAS catalog lookup, using FUMA to investigate the overlap of genes with other common traits[71] (Supplementary Fig. 12). Refractive error and hyperopia were replicated significantly after correction for multiple testing (adjusted P value $= 1.44 \times 10^{-52}$ and 9.34×10^{-9}, respectively). We found significant overlap with 74 other traits, of which height (adjusted P value $= 1.11 \times 10^{-10}$), obesity (adjusted $P = 1.38 \times 10^{-10}$) and body mass index (adjusted $P = 4.05 \times 10^{-7}$) were most important. Ocular diseases significantly associated were glaucoma (optic cup area and intraocular pressure, adjusted $P = 2.69 \times 10^{-5}$ and 3.01×10^{-5}, respectively) and age-related macular degeneration (adjusted $P = 1.27 \times 10^{-3}$).

Discussion

Myopia may become the leading cause of blindness worldwide in the near future, which suggests a grim outlook for which current counteractions remain insufficient[11,72]. To improve understanding of the genetic landscape and biology of refractive error, we conducted a large GWAS meta-analysis in 160,420 participants of mixed ancestry with replication in 95,505 participants. This study led to the identification of 139 independent susceptibility loci through single-variant analysis and 22 additional loci through post-GWAS methods, representing a fourfold increase in refractive-error genes. Most annotated genes were found to be expressed in the human posterior segment of the eye. Using in silico analysis, we identified significant biological pathways, of which retinal cell physiology, light processing and, specifically, glutamate receptor signaling were the most prominent mechanisms. Our integrated bioinformatic approach highlighted known ocular functionality for many genes.

To ensure the robustness of our genetic associations, we included studies of various designs and populations; sought replication in an independent cohort of significant sample size; and stringently accounted for population stratification by performing genomic control at all stages of the meta-analysis[73]. We combined studies with outcomes based on actual refractive-error measurements, as well as on the self-reported age of myopia onset, and found the direction of effect of the associated variants, as well as their effect size, to be highly consistent. Combining two different outcome measures may appear unconventional, but age of onset and refractive error have been shown to be very tightly correlated[11,28,74,75]. Moreover, the high genetic correlation (93%) of common SNPs between the two phenotypes underscores their similarity. The most compelling evidence was provided by replication of 86% of the discovered variants in the independent UKEV data, which also used conventional refractive-error measurements. This robustness indicates that both phenotypic outcomes can be used to capture a shared source of genetic variation. In addition, we found transancestral replication of significant loci and a high correlation of genetic effects of common variants in Europeans and Asians. Our findings support a largely shared genetic predisposition to refractive error and myopia in the two ancestries, although ancestry-specific allelic effects may exist. The low heritability estimate in Asians may be partly explained by the low representation of this ancestral group in our study sample; alternatively, it may imply that environmental factors explain a greater proportion of the phenotypic risk and recent rise in myopia prevalence in this ancestry group[76].

Limitations of our study were the possibility of false-negative findings due to genomic control and underrepresentation of studies including individuals of Asian ancestry. The heterogeneity of the observed effect estimates was large for several associated variants, but this result was not unexpected, given the large number of collaborating studies with varying methodology.

Although neurotransmission was a previously suggested pathway[26,27], our current pathway analyses provide more in-depth insights into the retinal circuitry driving refractive error. DEPICT identified 'thin retinal outer nuclear layer', 'detection of light stimulus' and 'nonmotile primary cilium' as the most important meta-gene sets. These are the main characteristics of photoreceptors, which are located in the outer retina and contain cilia. These photosensitive cells drive the phototransduction cascade in response to light, which in turn induces visual information processing. IPA indicated 'glutamate receptor signaling' as the most significant pathway. Glutamate is released by photoreceptors and determines conductance of retinal signaling to the ON and OFF bipolar cells[77]. Our functional gene lookups provide evidence that rod (*CLU*) as well as cone (*GNB3*) bipolar cells play a role. Together, these findings strongly suggest that light response and light processing in the retina are initiating factors leading to refractive error.

The genetic association with light-dependent pathways may also be linked to the well-established protective effect of outdoor exposure on myopia. We found evidence suggesting a genetic association with *DRD1*. The dopaminergic pathway has been studied extensively in animal models for its role in controlling eye growth in response to light[65,67,78–87]. *DRD1* has been found to be a mediator in this process, because bright light increases DRD1 activity in the bipolar ON pathway, and diminishes form-deprivation myopia in mice. Blockage of DRD1 reverses this inhibitory effect[88]. We did not find evidence of direct involvement of other genes in the dopamine pathway, but *GNB3* may be an indirect modifier, because it is a molecule involved in dopamine downstream signaling and has been shown to influence the availability of the dopamine transporter DAT[89]. Although it is a promising target for therapy, further evidence of *DRD1* in human myopiagenesis is warranted.

Novel pathways implicated by the newly identified genes are anterior-segment morphology (*TCF7L2*, *VIPR2* and *MAF*) and angiogenesis (*FLT1*). In addition, the high number of variants residing near genes encoding small RNAs suggests that post-transcriptional regulation is an important mechanism, because these RNAs are known to play a distinct and central regulatory role in cells[90]. These findings should serve as leads for future studies performing detailed mapping of cellular networks as well as for functional studies on genes that have been implicated in ocular phenotypes, that have protein-altering variants and that are proven drug targets.

Our evaluation of shared genetics between refractive error and other disease-relevant phenotypes highlighted overlap with anthropometric traits such as height, obesity and body mass index. These findings may provide valuable additional clues regarding the phenotypic outcomes of perturbations of some of the networks identified.

Our genetic observations add credence to the current notion that refractive errors are caused by a retina-to-sclera signaling cascade that induces scleral remodeling in response to light stimuli. The concept of this cascade originates from various animal models showing that form deprivation, retinal defocus and contrast, ambient light and wavelength influence eye growth in young animals[91–93]. The cell-specific moieties in this putative signaling cascade in humans are largely unknown, although animal models have implicated GABA, dopamine, all-*trans* retinoic acid and TGF-β (refs [65,87,94,95]). Our study provides a large number of new molecular candidates for this

cascade and clearly implicates a wide range of neuronal cell types in the retina, the RPE, the vascular endothelium and components of the extracellular matrix. The many interprotein relationships exemplify the complexity of eye growth and provide a challenge to developing strategies to prevent pathological eye elongation.

In conclusion, by using a cross-ancestry design in a large study population on common refractive errors, we identified numerous novel loci and pathways involved in eye growth. Our multidisciplinary approach incorporating GWAS data with in silico analyses and expression experiments provides an example for the design of future genetic studies for complex traits. Additional genetic insights into refractive errors will be gained by increasing sample size and genotyping depth; by performing family studies to identify rare alleles with large effects; and by evaluating population extremes. Our list of plausible genes and pathways provides a plethora of data for future studies focusing on gene–environment interaction and on translation of GWAS findings into starting points for therapy.

URLs. LDSC, https://github.com/bulik/ldsc/; Popcorn, https://github.com/brielin/Popcorn/; Online Mendelian Inheritance in Man (OMIM), http://omim.org/; wANNOVAR, http://wannovar.wglab.org/; PolyPhen-2, http://genetics.bwh.harvard.edu/pph2/; SIFT, http://sift.jcvi.org/www/SIFT_aligned_seqs_submit.html; MutationTaster, http://www.mutationtaster.org/; IPA, https://www.qiagenbioinformatics.com/products/ingenuity-pathway-analysis/; 1000 Genomes Project (release 2 May 2013), ftp.1000genomes.ebi.ac.uk; UCSC Genome Browser, https://genome.ucsc.edu/.

Methods

Methods, including statements of data availability and any associated accession codes and references, are available at https://doi.org/10.1038/s41588-018-0127-7.

Received: 22 May 2017; Accepted: 26 March 2018;
Published online: 28 May 2018

References

1. Pan, C. W., Ramamurthy, D. & Saw, S. M. Worldwide prevalence and risk factors for myopia. *Ophthalmic Physiol. Opt.* **32**, 3–16 (2012).
2. Morgan, I. G. What public policies should be developed to deal with the epidemic of myopia? *Optom. Vis. Sci.* **93**, 1058–1060 (2016).
3. Morgan, I. & Rose, K. How genetic is school myopia? *Prog. Retin. Eye Res.* **24**, 1–38 (2005).
4. Morgan, I. G., Ohno-Matsui, K. & Saw, S. M. Myopia. *Lancet* **379**, 1739–1748 (2012).
5. Williams, K. M. et al. Increasing prevalence of myopia in Europe and the impact of education. *Ophthalmology* **122**, 1489–1497 (2015).
6. Williams, K. M. et al. Prevalence of refractive error in Europe: the European Eye Epidemiology (E(3)) Consortium. *Eur. J. Epidemiol.* **30**, 305–315 (2015).
7. Vongphanit, J., Mitchell, P. & Wang, J. J. Prevalence and progression of myopic retinopathy in an older population. *Ophthalmology* **109**, 704–711 (2002).
8. Seet, B. et al. Myopia in Singapore: taking a public health approach. *Br. J. Ophthalmol.* **85**, 521–526 (2001).
9. Smith, T. S., Frick, K. D., Holden, B. A., Fricke, T. R. & Naidoo, K. S. Potential lost productivity resulting from the global burden of uncorrected refractive error. *Bull. World Health Organ.* **87**, 431–437 (2009).
10. Verhoeven, V. J. et al. Visual consequences of refractive errors in the general population. *Ophthalmology* **122**, 101–109 (2015).
11. Tideman, J. W. et al. Association of axial length with risk of uncorrectable visual impairment for Europeans with myopia. *JAMA Ophthalmol.* **134**, 1355–1363 (2016).
12. Flitcroft, D. I. The complex interactions of retinal, optical and environmental factors in myopia aetiology. *Prog. Retin. Eye Res.* **31**, 622–660 (2012).
13. Nakanishi, H. et al. A genome-wide association analysis identified a novel susceptible locus for pathological myopia at 11q24.1. *PLoS Genet.* **5**, e1000660 (2009).
14. Lam, C. Y. et al. A genome-wide scan maps a novel high myopia locus to 5p15. *Invest. Ophthalmol. Vis. Sci.* **49**, 3768–3778 (2008).
15. Stambolian, D. et al. Meta-analysis of genome-wide association studies in five cohorts reveals common variants in RBFOX1, a regulator of tissue-specific splicing, associated with refractive error. *Hum. Mol. Genet.* **22**, 2754–2764 (2013).
16. Fan, Q. et al. Genetic variants on chromosome 1q41 influence ocular axial length and high myopia. *PLoS Genet.* **8**, e1002753 (2012).
17. Fan, Q. et al. Meta-analysis of gene-environment-wide association scans accounting for education level identifies additional loci for refractive error. *Nat. Commun.* **7**, 11008 (2016).
18. Cheng, C. Y. et al. Nine loci for ocular axial length identified through genome-wide association studies, including shared loci with refractive error. *Am. J. Hum. Genet.* **93**, 264–277 (2013).
19. Shi, Y. et al. Exome sequencing identifies ZNF644 mutations in high myopia. *PLoS Genet.* **7**, e1002084 (2011).
20. Shi, Y. et al. Genetic variants at 13q12.12 are associated with high myopia in the Han Chinese population. *Am. J. Hum. Genet.* **88**, 805–813 (2011).
21. Li, Y. J. et al. Genome-wide association studies reveal genetic variants in CTNND2 for high myopia in Singapore Chinese. *Ophthalmology* **118**, 368–375 (2011).
22. Li, Z. et al. A genome-wide association study reveals association between common variants in an intergenic region of 4q25 and high-grade myopia in the Chinese Han population. *Hum. Mol. Genet.* **20**, 2861–2868 (2011).
23. Liu, J. & Zhang, H. X. Polymorphism in the 11q24.1 genomic region is associated with myopia: a comprehensive genetic study in Chinese and Japanese populations. *Mol. Vis.* **20**, 352–358 (2014).
24. Tran-Viet, K. N. et al. Mutations in SCO2 are associated with autosomal-dominant high-grade myopia. *Am. J. Hum. Genet.* **92**, 820–826 (2013).
25. Aldahmesh, M. A. et al. Mutations in LRPAP1 are associated with severe myopia in humans. *Am. J. Hum. Genet.* **93**, 313–320 (2013).
26. Verhoeven, V. J. et al. Genome-wide meta-analyses of multiancestry cohorts identify multiple new susceptibility loci for refractive error and myopia. *Nat. Genet.* **45**, 314–318 (2013).
27. Kiefer, A. K. et al. Genome-wide analysis points to roles for extracellular matrix remodeling, the visual cycle, and neuronal development in myopia. *PLoS Genet.* **9**, e1003299 (2013).
28. Wojciechowski, R. & Hysi, P. G. Focusing in on the complex genetics of myopia. *PLoS Genet.* **9**, e1003442 (2013).
29. 1000 Genomes Project Consortium. et al. A global reference for human genetic variation. *Nature* **526**, 68–74 (2015).
30. Bulik-Sullivan, B. K. et al. LD Score regression distinguishes confounding from polygenicity in genome-wide association studies. *Nat. Genet.* **47**, 291–295 (2015).
31. Yang, J. et al. Genomic inflation factors under polygenic inheritance. *Eur. J. Hum. Genet.* **19**, 807–812 (2011).
32. Watanabe, K., Taskesen, E., van Bochoven, A. & Posthuma, D. Functional mapping and annotation of genetic associations with FUMA. *Nat. Commun.* **8**, 1826 (2017).
33. Plotnikov, D., Guggenheim, J. & The UK Biobank Eye and Vision Consortium. Is a large eye size a risk factor for myopia? A Mendelian randomization study. https://www.biorxiv.org/content/early/2017/12/29/240283/ (2017).
34. Hsu, F. et al. The UCSC Known Genes. *Bioinformatics* **22**, 1036–1046 (2006).
35. Adzhubei, I. A. et al. A method and server for predicting damaging missense mutations. *Nat. Methods* **7**, 248–249 (2010).
36. Ng, P. C. & Henikoff, S. SIFT: predicting amino acid changes that affect protein function. *Nucleic Acids Res.* **31**, 3812–3814 (2003).
37. Kelly, M. P. Does phosphodiesterase 11A (PDE11A) hold promise as a future therapeutic target? *Curr. Pharm. Des.* **21**, 389–416 (2015).
38. Kumar, P., Henikoff, S. & Ng, P. C. Predicting the effects of coding non-synonymous variants on protein function using the SIFT algorithm. *Nat. Protoc.* **4**, 1073–1081 (2009).
39. Mathe, E. et al. Computational approaches for predicting the biological effect of p53 missense mutations: a comparison of three sequence analysis based methods. *Nucleic Acids Res.* **34**, 1317–1325 (2006).
40. Tavtigian, S. V. et al. Comprehensive statistical study of 452 BRCA1 missense substitutions with classification of eight recurrent substitutions as neutral. *J. Med. Genet.* **43**, 295–305 (2006).
41. Bakshi, A. et al. Fast set-based association analysis using summary data from GWAS identifies novel gene loci for human complex traits. *Sci. Rep.* **6**, 32894 (2016).
42. Ferreira, M. A. et al. Gene-based analysis of regulatory variants identifies 4 putative novel asthma risk genes related to nucleotide synthesis and signaling. *J. Allergy Clin. Immunol.* **139**, 1148–1157 (2017).
43. Pickrell, J. K. Joint analysis of functional genomic data and genome-wide association studies of 18 human traits. *Am. J. Hum. Genet.* **94**, 559–573 (2014).
44. Purcell, S. M. et al. Common polygenic variation contributes to risk of schizophrenia and bipolar disorder. *Nature* **460**, 748–752 (2009).
45. Verhoeven, V. J. et al. Large scale international replication and meta-analysis study confirms association of the 15q14 locus with myopia. The CREAM consortium. *Hum. Genet.* **131**, 1467–1480 (2012).

46. Finucane, H. K. et al. Partitioning heritability by functional annotation using genome-wide association summary statistics. *Nat. Genet.* **47**, 1228–1235 (2015).
47. Brown, B. C., Asian Genetic Epidemiology Network Type 2 Diabetes Consortium, Ye, C. J., Price, A. L. & Zaitlen, N. Transethnic genetic-correlation estimates from summary statistics. *Am. J. Hum. Genet.* **99**, 76–88 (2016).
48. Pers, T. H. et al. Biological interpretation of genome-wide association studies using predicted gene functions. *Nat. Commun.* **6**, 5890 (2015).
49. Fritsche, L. G. et al. A large genome-wide association study of age-related macular degeneration highlights contributions of rare and common variants. *Nat. Genet.* **48**, 134–143 (2016).
50. Ritchey, E. R. et al. Vision-guided ocular growth in a mutant chicken model with diminished visual acuity. *Exp. Eye Res.* **102**, 59–69 (2012).
51. Vincent, A. et al. Biallelic mutations in GNB3 cause a unique form of autosomal-recessive congenital stationary night blindness. *Am. J. Hum. Genet.* **98**, 1011–1019 (2016).
52. Blake, J. A. et al. Mouse Genome Database (MGD)-2017: community knowledge resource for the laboratory mouse. *Nucleic Acids Res.* **45**, D723–D729 (2017).
53. Nikonov, S. S. et al. Cones respond to light in the absence of transducin β subunit. *J. Neurosci.* **33**, 5182–5194 (2013).
54. Stone, E. M. et al. A single EFEMP1 mutation associated with both Malattia Leventinese and Doyne honeycomb retinal dystrophy. *Nat. Genet.* **22**, 199–202 (1999).
55. Mackay, D. S., Bennett, T. M. & Shiels, A. Exome sequencing identifies a missense variant in EFEMP1 co-segregating in a family with autosomal dominant primary open-angle glaucoma. *PLoS One* **10**, e0132529 (2015).
56. Springelkamp, H. et al. ARHGEF12 influences the risk of glaucoma by increasing intraocular pressure. *Hum. Mol. Genet.* **24**, 2689–2699 (2015).
57. Haeseleer, F. et al. Essential role of Ca^{2+}-binding protein 4, a Cav1.4 channel regulator, in photoreceptor synaptic function. *Nat. Neurosci.* **7**, 1079–1087 (2004).
58. Littink, K. W. et al. A novel homozygous nonsense mutation in CABP4 causes congenital cone-rod synaptic disorder. *Invest. Ophthalmol. Vis. Sci.* **50**, 2344–2350 (2009).
59. Grimes, W. N., Li, W., Chávez, A. E. & Diamond, J. S. BK channels modulate pre- and postsynaptic signaling at reciprocal synapses in retina. *Nat. Neurosci.* **12**, 585–592 (2009).
60. Keckeis, S., Reichhart, N., Roubeix, C. & Strauß, O. Anoctamin2 (TMEM16B) forms the Ca^{2+}-activated Cl^- channel in the retinal pigment epithelium. *Exp. Eye Res.* **154**, 139–150 (2017).
61. Prasanna, G., Narayan, S., Krishnamoorthy, R. R. & Yorio, T. Eyeing endothelins: a cellular perspective. *Mol. Cell. Biochem.* **253**, 71–88 (2003).
62. Yamashita, T. et al. Essential and synergistic roles of RP1 and RP1L1 in rod photoreceptor axoneme and retinitis pigmentosa. *J. Neurosci.* **29**, 9748–9760 (2009).
63. Davidson, A. E. et al. RP1L1 variants are associated with a spectrum of inherited retinal diseases including retinitis pigmentosa and occult macular dystrophy. *Hum. Mutat.* **34**, 506–514 (2013).
64. Hawthorne, F. et al. Association mapping of the high-grade myopia MYP3 locus reveals novel candidates UHRF1BP1L, PTPRR, and PPFIA2. *Invest. Ophthalmol. Vis. Sci.* **54**, 2076–2086 (2013).
65. Feldkaemper, M. & Schaeffel, F. An updated view on the role of dopamine in myopia. *Exp. Eye Res.* **114**, 106–119 (2013).
66. Paul, M. L., Graybiel, A. M., David, J. C. & Robertson, H. A. D1-like and D2-like dopamine receptors synergistically activate rotation and c-fos expression in the dopamine-depleted striatum in a rat model of Parkinson's disease. *J. Neurosci.* **12**, 3729–3742 (1992).
67. Stone, R. A., Lin, T., Laties, A. M. & Iuvone, P. M. Retinal dopamine and form-deprivation myopia. *Proc. Natl. Acad. Sci. USA* **86**, 704–706 (1989).
68. Gardner, M., Bertranpetit, J. & Comas, D. Worldwide genetic variation in dopamine and serotonin pathway genes: implications for association studies. *Am. J. Med. Genet. B. Neuropsychiatr. Genet.* **147B**, 1070–1075 (2008).
69. D'Souza, U. M. & Craig, I. W. Functional polymorphisms in dopamine and serotonin pathway genes. *Hum. Mutat.* **27**, 1–13 (2006).
70. Beaulieu, J. M. & Gainetdinov, R. R. The physiology, signaling, and pharmacology of dopamine receptors. *Pharmacol. Rev.* **63**, 182–217 (2011).
71. MacArthur, J. et al. The new NHGRI-EBI Catalog of published genome-wide association studies (GWAS Catalog). *Nucleic Acids Res.* **45**, D896–D901 (2017).
72. Holden, B. A. et al. Global prevalence of myopia and high myopia and temporal trends from 2000 through 2050. *Ophthalmology* **123**, 1036–1042 (2016).
73. Cardon, L. R. & Palmer, L. J. Population stratification and spurious allelic association. *Lancet* **361**, 598–604 (2003).
74. Chua, S. Y. et al. Age of onset of myopia predicts risk of high myopia in later childhood in myopic Singapore children. *Ophthalmic Physiol. Opt.* **36**, 388–394 (2016).
75. Williams, K. M. et al. Age of myopia onset in a British population-based twin cohort. *Ophthalmic Physiol. Opt.* **33**, 339–345 (2013).
76. Dolgin, E. The myopia boom. *Nature* **519**, 276–278 (2015).
77. Connaughton, V. Glutamate and glutamate receptors in the vertebrate retina. In: H. Kolb et al. eds. *Webvision: The Organization of the Retina and Visual System* (Webvision, Salt Lake City, UT, USA, 1995).
78. Hung, G. K., Mahadas, K. & Mohammad, F. Eye growth and myopia development: unifying theory and Matlab model. *Comput. Biol. Med.* **70**, 106–118 (2016).
79. Norton, T. T. What do animal studies tell us about the mechanism of myopia-protection by light? *Optom. Vis. Sci.* **93**, 1049–1051 (2016).
80. Weiss, S. & Schaeffel, F. Diurnal growth rhythms in the chicken eye: relation to myopia development and retinal dopamine levels. *J. Comp. Physiol. A* **172**, 263–270 (1993).
81. Stone, R. A., Lin, T., Iuvone, P. M. & Laties, A. M. Postnatal control of ocular growth: dopaminergic mechanisms. *Ciba Found. Symp.* **155**, 45–62 (1990).
82. Morgan, I. G. The biological basis of myopic refractive error. *Clin. Exp. Optom.* **86**, 276–288 (2003).
83. Li, X. X., Schaeffel, F., Kohler, K. & Zrenner, E. Dose-dependent effects of 6-hydroxy dopamine on deprivation myopia, electroretinograms, and dopaminergic amacrine cells in chickens. *Vis. Neurosci.* **9**, 483–492 (1992).
84. Iuvone, P. M., Tigges, M., Stone, R. A., Lambert, S. & Laties, A. M. Effects of apomorphine, a dopamine receptor agonist, on ocular refraction and axial elongation in a primate model of myopia. *Invest. Ophthalmol. Vis. Sci.* **32**, 1674–1677 (1991).
85. Ashby, R., McCarthy, C. S., Maleszka, R., Megaw, P. & Morgan, I. G. A muscarinic cholinergic antagonist and a dopamine agonist rapidly increase ZENK mRNA expression in the form-deprived chicken retina. *Exp. Eye Res.* **85**, 15–22 (2007).
86. Ashby, R. Animal studies and the mechanism of myopia-protection by light? *Optom. Vis. Sci.* **93**, 1052–1054 (2016).
87. Rymer, J. & Wildsoet, C. F. The role of the retinal pigment epithelium in eye growth regulation and myopia: a review. *Vis. Neurosci.* **22**, 251–261 (2005).
88. Chen, S. et al. Bright light suppresses form-deprivation myopia development with activation of dopamine D1 receptor signaling in the ON pathway in retina. *Invest. Ophthalmol. Vis. Sci.* **58**, 2306–2316 (2017).
89. Chen, P. S. et al. Effects of C825T polymorphism of the GNB3 gene on availability of dopamine transporter in healthy volunteers: a SPECT study. *Neuroimage* **56**, 1526–1530 (2011).
90. Scott, M. S. & Ono, M. From snoRNA to miRNA: dual function regulatory non-coding RNAs. *Biochimie* **93**, 1987–1992 (2011).
91. McFadden, S. A. Understanding and treating myopia: what more we need to know and future research priorities. *Optom. Vis. Sci.* **93**, 1061–1063 (2016).
92. Smith, E. L. III, Hung, L. F. & Arumugam, B. Visual regulation of refractive development: insights from animal studies. *Eye (Lond.)* **28**, 180–188 (2014).
93. Zhang, Y. & Wildsoet, C. F. RPE and choroid mechanisms underlying ocular growth and myopia. *Prog. Mol. Biol. Transl. Sci.* **134**, 221–240 (2015).
94. Harper, A. R. & Summers, J. A. The dynamic sclera: extracellular matrix remodeling in normal ocular growth and myopia development. *Exp. Eye Res.* **133**, 100–111 (2015).
95. Summers, J. A. The choroid as a sclera growth regulator. *Exp. Eye Res.* **114**, 120–127 (2013).

Acknowledgements

We gratefully thank all study participants, their relatives and the staff at the recruitment centers for their invaluable contributions. We thank all contributors to the CREAM Consortium, 23andMe and UKEV for their generosity in sharing data and help in the production of this publication. Funding for this particular GWAS mega-analysis was provided by the European Research Council (ERC) under the European Union's Horizon 2020 Research and Innovation Programme (grant 648268), the Netherlands Organisation for Scientific Research (NWO, grant 91815655) and the National Eye Institute (grant R01EY020483). Funding agencies that facilitated the execution of the individual studies are acknowledged in the Supplementary Note.

Author contributions

M.S.T., V.J.M.V., S.M., J.A.G., A.I.I., R.W., P.G.H., A.I.I. and E.M.v.L. performed the analyses. C.C.W.K., V.J.M.V., M.S.T., R.W., J.A.G. and S.M. drafted the manuscript, and C.J.H., P.G.H., A.P.K., C.M.v.D., D.S., E.M.v.L., J.E.B.-W., J.Y.T., N.A.F., Q.F., S.-M.S. and V.V. critically reviewed the manuscript. A.N., A.P.K., A.T., C.B., C. Gieger, C.L.S., C.-Y.C., G. Biino, G.C.-P., I.R., J.E.B.W., J.E.H., J. S. Ried, J.W., J.X., K.M.W., K.Y., P.M.C., S.M.H., M.S.T., N.A.F., N.E., P.C., P. Gharahkhani, P.K.J., Q.F., R. Höhn, R.L.S., R.P.I., R.W., T.H., T.-H.S.-A., T.Z., V.V., W.-Y.S., W.Z., X.L.S., Y.C.T., Y.S. and Y.Y.T. performed data analysis for the individual studies; A.D.P., A.G.U., A.T., A.W.H., B.E.K.K., C.C.W.K., C.D., C. Grazal, C.H., C.J.H., C.W., C.-Y.C., D.A.M., F.R., G. Bencic, H.M.-H., J.A.G., J.B.J., J.E.B.-W., J.E.C., J.F.W., J.H.L., J.R.V., J. S. Rahi, J. S. Ried, J.Y.T., K.Y., M.A.M.-S.,

N.G.M., N.P., O. Polašek, O. Pärssinen, O.T.R., P. Gupta, P.J.F., P.M., P.N.B., R.K., S.K.I., S.-M.S., T.L., T.M., W.Z., Y.C.T. and Y.X.W. contributed to data assembly. A.A.B.B., A.W., C. Grazal, D.S., K.N.W., S.W.T. and T.L.Y. performed expression experiments, and M.S.T., A.A.B.B., P.J.v.d.S. and R. Hask performed in silico pathway analyses. C.C.W.K. and C.J.H. conceived and designed the outline of the current report, and supervised conduction of experiments and analyses jointly with A.M., A.H., A.W.H., C.D., C.H., C.J.H., C.M.v.D., C.W., C.-Y.C., D.A.M., D.S., E.-S.T., F.M., G. Biino, I.R., J.A.G., J.B.J., J.E.B.-W., J.E.C., J.F.W., J.H.L., J.R.V., J.Y.T., N.A., N.A.F., N.P., O. Pärssinen, O.T.R., P.J.F., P.N.B., S.K.I., S.-M.S., T.L., T.Y.W., T.L.Y., V.V., Y.X.W. and Y.Y.T. M.P.C. analyzed the data and performed statistical analyses. The 23andMe research team, CREAM and the UK Biobank Eye and Vision Consortium contributed reagents/materials/analysis tools and performed statistical analyses.

Competing interests

N.A.F., N.E., J.Y.T. and the 23andMe Research Team are current or former employees of 23andMe, Inc., and hold stock or stock options in 23andMe. J.B.J. is a patent holder with Biocompatibles UK Ltd. (Franham, Surrey, UK) (Title: Treatment of eye diseases using encapsulated cells encoding and secreting neuroprotective factor and /or anti-angiogenic factor; international patent no. 20120263794) and is included in a patent application with University of Heidelberg (Heidelberg, Germany) (Title: Agents for use in the therapeutic or prophylactic treatment of myopia or hyperopia; European patent no. 3 070 101). The other authors declare no competing financial interests.

Additional information

Supplementary information is available for this paper at https://doi.org/10.1038/s41588-018-0127-7.

Reprints and permissions information is available at www.nature.com/reprints.

Correspondence and requests for materials should be addressed to C.C.W.K.

Publisher's note: Springer Nature remains neutral with regard to jurisdictional claims in published maps and institutional affiliations.

[1]Department of Ophthalmology, Erasmus Medical Center, Rotterdam, The Netherlands. [2]Department of Epidemiology, Erasmus Medical Center, Rotterdam, The Netherlands. [3]Department of Epidemiology and Medicine, Johns Hopkins Bloomberg School of Public Health, Baltimore, MD, USA. [4]Computational and Statistical Genomics Branch, National Human Genome Research Institute, National Institutes of Health, Bethesda, MD, USA. [5]Wilmer Eye Institute, Johns Hopkins Medical Institutions, Baltimore, MD, USA. [6]Section of Academic Ophthalmology, School of Life Course Sciences, King's College London, London, UK. [7]23andMe, Inc., Mountain View, CA, USA. [8]Department of Clinical Genetics, Erasmus Medical Center, Rotterdam, The Netherlands. [9]Department of Ophthalmology and Visual Sciences, University of Wisconsin–Madison, Madison, WI, USA. [10]Centre for Quantitative Medicine, DUKE–National University of Singapore, Singapore, Singapore. [11]Department of Public Health and Primary Care, University of Cambridge, Cambridge, UK. [12]NIHR Biomedical Research Centre, Moorfields Eye Hospital NHS Foundation Trust and UCL Institute of Ophthalmology, London, UK. [13]Ocular Epidemiology Research Group, Singapore Eye Research Institute, Singapore National Eye Centre, Singapore, Singapore. [14]Department of Ophthalmology, University Hospital Bern, Inselspital, University of Bern, Bern, Switzerland. [15]Department of Ophthalmology, University Medical Center Mainz, Mainz, Germany. [16]Department of Ophthalmology and Visual Sciences, Kyoto University Graduate School of Medicine, Kyoto, Japan. [17]Department of Ophthalmology, University of Pennsylvania, Philadelphia, PA, USA. [18]Estonian Genome Center, University of Tartu, Tartu, Estonia. [19]Department of Ophthalmology, University of Helsinki and Helsinki University Hospital, Helsinki, Finland. [20]Department of Public Health, University of Helsinki, Helsinki, Finland. [21]Department of Ophthalmology, Medical Faculty Mannheim of the Ruprecht-Karls-University of Heidelberg, Mannheim, Germany. [22]Beijing Institute of Ophthalmology, Beijing Key Laboratory of Ophthalmology and Visual Sciences, Beijing Tongren Eye Center, Beijing Tongren Hospital, Capital Medical University, Beijing, China. [23]Centre for Eye Research Australia, Ophthalmology, Department of Surgery, University of Melbourne, Royal Victorian Eye and Ear Hospital, Melbourne, Victoria, Australia. [24]Department of Ophthalmology, Centre for Vision Research, Westmead Institute for Medical Research, University of Sydney, Sydney, New South Wales, Australia. [25]Program in Genetics and Genome Biology, Hospital for Sick Children and University of Toronto, Toronto, Ontario, Canada. [26]School of Optometry & Vision Sciences, Cardiff University, Cardiff, UK. [27]Department of Population Health Sciences, Bristol Medical School, Bristol, UK. [28]Department of Statistics and Applied Probability, National University of Singapore, Singapore, Singapore. [29]Saw Swee Hock School of Public Health, National University Health Systems, National University of Singapore, Singapore, Singapore. [30]Department of Health Service Research, Singapore Eye Research Institute, Singapore National Eye Centre, Singapore, Singapore. [31]Statistics Support Platform, Singapore Eye Research Institute, Singapore National Eye Centre, Singapore, Singapore. [32]Life Sciences Institute, National University of Singapore, Singapore, Singapore. [33]MRC Human Genetics Unit, MRC Institute of Genetics & Molecular Medicine, University of Edinburgh, Edinburgh, UK. [34]Faculty of Medicine, University of Split, Split, Croatia. [35]Department of Ophthalmology, Sisters of Mercy University Hospital, Zagreb, Croatia. [36]Centre for Global Health Research, Usher Institute for Population Health Sciences and Informatics, University of Edinburgh, Edinburgh, UK. [37]A list of members and affiliations appears at the end of the paper. [38]Center for Genomic Medicine, Kyoto University Graduate School of Medicine, Kyoto, Japan. [39]Clinic for General and Interventional Cardiology, University Heart Center Hamburg, Hamburg, Germany. [40]Department of Bioinformatics, Erasmus Medical Center, Rotterdam, The Netherlands. [41]Department of Clinical Genetics, Academic Medical Center, Amsterdam, The Netherlands. [42]Department of Clinical Genetics, VU University Medical Center, Amsterdam, The Netherlands. [43]Department of Population and Quantitative Health Sciences, Case Western Reserve University, Cleveland, OH, USA. [44]Department of Ophthalmology and Visual Sciences, Case Western Reserve University and University Hospitals Eye Institute, Cleveland, OH, USA. [45]Department of Genetics, Case Western Reserve University, Cleveland, OH, USA. [46]Department of Epidemiology, Harvard T.H. Chan School of Public Health, Boston, MA, USA. [47]Netherlands Consortium for Healthy Ageing, Netherlands Genomics Initiative, The Hague, The Netherlands. [48]Department of Internal Medicine, Erasmus Medical Center, Rotterdam, The Netherlands. [49]Department of Clinical Chemistry, Finnish Cardiovascular Research Center–Tampere, Faculty of Medicine and Life Sciences, University of Tampere, Tampere, Finland. [50]Department of Clinical Chemistry, Fimlab Laboratories, University of Tampere, Tampere, Finland. [51]Research Centre of Applied and Preventive Cardiovascular Medicine, University of Turku, Turku, Finland. [52]Department of Clinical Physiology and Nuclear Medicine, Turku University Hospital, Turku, Finland. [53]Institute of Molecular Genetics, National Research Council of Italy, Pavia, Italy. [54]Institute for Maternal and Child Health–IRCCS 'Burlo Garofolo', Trieste, Italy. [55]Department of Medical and Molecular Genetics, Indiana University, School of Medicine, Indianapolis, IN, USA. [56]Statistical Genetics, QIMR Berghofer Medical Research Institute, Brisbane, Queensland, Australia. [57]Genetic Epidemiology, QIMR Berghofer Medical Research Institute, Brisbane, Queensland, Australia. [58]Department of Ophthalmology, Flinders University, Adelaide, South Australia, Australia. [59]Department of Twin Research and Genetic Epidemiology, King's College London, London, UK. [60]Great Ormond Street Institute of Child Health, University College London, London, UK. [61]Ulverscroft Vision Research Group, University College London, London, UK. [62]Université de Bordeaux, Inserm, Bordeaux Population Health Research Center, team LEHA, UMR 1219, F-33000 Bordeaux, France. [63]Institut Pasteur de Lille, Lille, France. [64]Inserm, U1167, RID-AGE–Risk factors and molecular determinants of aging-related diseases, Lille, France. [65]Université de Lille, U1167–Excellence Laboratory LabEx DISTALZ, Lille, France. [66]Research Unit of Molecular Epidemiology, Institute of Epidemiology, Helmholtz Zentrum München–German Research Center for Environmental Health, Neuherberg, Germany. [67]Department of Ophthalmology, Academic Medical Center, Amsterdam, The Netherlands. [68]Netherlands Institute for Neurosciences (NIN-KNAW), Amsterdam, The Netherlands. [69]Institute of Human Genetics, Helmholtz Zentrum München, Neuherberg, Germany. [70]Institute of Human Genetics, Klinikum rechts der Isar, Technische Universität München, Munich, Germany. [71]Academic Medicine Research Institute, Singapore, Singapore. [72]Retino Center, Singapore National Eye Centre, Singapore, Singapore. [73]Department of Ophthalmology, Menzies Institute of Medical Research, University of Tasmania, Hobart, Tasmania, Australia. [74]Centre for

Ophthalmology and Visual Science, Lions Eye Institute, University of Western Australia, Perth, Western Australia, Australia. [75]Department of Genetics, Genomics and Informatics, University of Tennessee Health Sciences Center, Memphis, TN, USA. [76]Department of Ophthalmology, Central Hospital of Central Finland, Jyväskylä, Finland. [77]Gerontology Research Center, Faculty of Sport and Health Sciences, University of Jyväskylä, Jyväskylä, Finland. [78]Myopia Research Group, Singapore Eye Research Institute, Singapore National Eye Centre, Singapore, Singapore. [79]Department of Ophthalmology, Radboud University Medical Center, Nijmegen, The Netherlands. [80]These authors contributed equally: Milly S. Tedja, Robert Wojciechowski, Pirro G. Hysi, Nicholas Eriksson, Nicholas A. Furlotte, Virginie J. M. Verhoeven. [81]These authors jointly supervised this work: Jeremy A. Guggenheim, Joyce Y. Tung, Christopher J. Hammond, Caroline C. W. Klaver. *e-mail: c.c.w.klaver@erasmusmc.nl

The CREAM Consortium

Tin Aung[82,83], Amutha B. Veluchamy[82,84], Kathryn P. Burdon[58], Harry Campbell[36], Li Jia Chen[85], Peng Chen[83], Wei Chen[86], Emily Chew[45], Margaret M. Deangelis[87], Xiaohu Ding[88], Angela Döring[66], David M. Evans[89,90], Sheng Feng[91], Brian Fleck[92], Rhys D. Fogarty[58], Jeremy R. Fondran[43], Maurizio Fossarello[93], Xiaobo Guo[88,94], Annet E. G. Haarman[1,2], Mingguang He[23,88], Laura D. Howe[90,95], Sarayut Janmahasatian[43], Vishal Jhanji[85], Mika Kähönen[96], Jaakko Kaprio[20,97], John P. Kemp[90], Kay-Tee Khaw[11], Chiea-Chuen Khor[29,83,87,98], Eva Krapohl[99], Jean-François Korobelnik[100,101], Kris Lee[9], Shi-Ming Li[22], Yi Lu[56], Robert N. Luben[11], Kari-Matti Mäkelä[49], George McMahon[90], Akira Meguro[102], Evelin Mihailov[18], Masahiro Miyake[16], Nobuhisa Mizuki[102], Margaux Morrison[87], Vinay Nangia[103], Konrad Oexle[104], Songhomitra Panda-Jonas[103], Chi Pui Pang[85], Mario Pirastu[105], Robert Plomin[99], Taina Rantanen[77], Maria Schache[23], Ilkka Seppälä[49], George D. Smith[90], Beate St Pourcain[90,106], Pancy O. Tam[85], J. Willem L. Tideman[1,2], Nicholas J. Timpson[90], Simona Vaccargiu[105], Zoran Vatavuk[35], Jie Jin Wang[23,24], Ningli Wang[22], Nick J. Wareham[107], Alan F. Wright[33], Liang Xu[22], Maurice K. H. Yap[108], Seyhan Yazar[74], Shea Ping Yip[109], Nagahisa Yoshimura[16], Alvin L. Young[9], Jing Hua Zhao[107] and Xiangtian Zhou[86]

23andMe Research Team

Michelle Agee[7], Babak Alipanahi[7], Adam Auton[7], Robert K. Bell[7], Katarzyna Bryc[7], Sarah L. Elson[7], Pierre Fontanillas[7], David A. Hinds[7], Jennifer C. McCreight[7], Karen E. Huber[7], Aaron Kleinman[7], Nadia K. Litterman[7], Matthew H. McIntyre[7], Joanna L. Mountain[7], Elizabeth S. Noblin[7], Carrie A. M. Northover[7], Steven J. Pitts[7], J. Fah Sathirapongsasuti[7], Olga V. Sazonova[7], Janie F. Shelton[7], Suyash Shringarpure[7], Chao Tian[7], Vladimir Vacic[7] and Catherine H. Wilson[7]

UK Biobank Eye and Vision Consortium

Tariq M. Aslam[110], Sarah A. Barman[111], Jenny H. Barrett[112], Paul N. Bishop[110], Peter Blows[12], Catey Bunce[113], Roxana O. Carare[114], Usha Chakravarthy[115], Michelle Chan[12], Sharon Chua[12], David Crabb[116], Alexander Day[12], Parul Desai[12], Bal Dhillon[117], Andrew D. Dick[118], Cathy A. Egan[12], Sarah Ennis[114], Marcus Fruttiger[12], John Gallacher[119], David F. Garway-Heath[12], Jane Gibson[114], Dan M. Gore[12], Alison Hardcastle[12], Simon P. Harding[120], Ruth E. Hogg[121], Pearse A. Keane[12], Peng Tee Khaw[12], Gerassimos Lascaratos[12], Andrew Lotery[122], Phil J. Luthert[12], Tom J. MacGillivray[123], Sarah L. Mackie[124], Keith R. Martin[125], Michelle McGaughey[126], Bernadette McGuinness[126], Gareth J. McKay[126], Martin McKibbin[127], Danny Mitry[12], Tony Moore[12], James E. Morgan[26], Zaynah A. Muthy[12], Eoin O'Sullivan[128], Chris Owen[129], Praveen J. Patel[12], Euan N. Paterson[126], Tunde Peto[115], Axel Petzold[130], Alicja R. Rudnicka[129], Jay E. Self[122,131], Sobha Sivaprasad[12], David H. W. Steel[132], Irene M. Stratton[133], Nicholas Strouthidis[12], Cathie L. M. Sudlow[134], Caroline Thaung[12], Dhanes Thomas[12], Emanuele Trucco[135], Adnan Tufail[12], Stephen A. Vernon[136], Ananth C. Viswanathan[12], Jayne V. Woodside[126], Max Yates[137], Jennifer L. Y. Yip[11] and Yalin Zheng[120]

[82]Singapore Eye Research Institute, Singapore National Eye Centre, Singapore, Singapore. [83]Department of Ophthalmology, National University Health Systems, National University of Singapore, Singapore, Singapore. [84]Duke-NUS Medical School, Singapore, Singapore, Singapore. [85]Department of Ophthalmology and Visual Sciences, Chinese University of Hong Kong, Hong Kong Eye Hospital, Kowloon, Hong Kong. [86]School of Ophthalmology and Optometry, Eye Hospital, Wenzhou Medical University, Wenzhou, China. [87]Department of Ophthalmology and Visual Sciences, John Moran Eye Center, University of Utah, Salt Lake City, UT, USA. [88]State Key Laboratory of Ophthalmology, Zhongshan Ophthalmic Center, Sun Yat-sen University, Guangzhou, China. [89]Translational Research Institute, University of Queensland Diamantina Institute, Brisbane, Queensland, Australia. [90]MRC Integrative Epidemiology Unit, University of Bristol, Bristol, UK. [91]Department of Pediatric Ophthalmology, Duke Eye Center For Human Genetics, Durham, NC, USA. [92]Princess Alexandra Eye Pavilion, Edinburgh, UK. [93]University Hospital 'San Giovanni di Dio', Cagliari, Italy. [94]Department of Statistical Science, School of Mathematics, Sun Yat-Sen University, Guangzhou, China. [95]School of Social and Community Medicine, University of Bristol, Bristol, UK. [96]Department of Clinical Physiology, Tampere University Hospital and School of Medicine, University of Tampere, Tampere, Finland. [97]Institute for Molecular Medicine Finland FIMM, HiLIFE Unit, University of Helsinki, Helsinki, Finland. [98]Division of Human Genetics, Genome Institute of Singapore, Singapore, Singapore. [99]MRC Social, Genetic and Developmental Psychiatry Centre, Institute of Psychiatry, Psychology & Neuroscience, King's College London, London, UK. [100]Université de Bordeaux, Bordeaux, France. [101]Institut National de la Santé Et de la Recherche Médicale (INSERM), Institut de Santé Publique d'Épidémiologie et de Développement (ISPED), Centre INSERM U897–Epidemiologie-Biostatistique, Bordeaux, France. [102]Department of Ophthalmology, Yokohama City University School of Medicine, Yokohama, Japan. [103]Suraj Eye Institute, Nagpur, Maharashtra, India. [104]Institute of Neurogenomics, Helmholtz Zentrum München, German Research Centre for Environmental Health, Neuherberg, Germany. [105]Institute of Genetic and Biomedic Research, National Research Council, Cagliari, Italy. [106]Max Planck Institute for Psycholinguistics, Nijmegen, The Netherlands. [107]MRC Epidemiology Unit, Institute of Metabolic Sciences, University of Cambridge, Cambridge, UK. [108]Centre for Myopia Research, School of Optometry, Hong Kong Polytechnic University, Hong Kong, Hong Kong. [109]Department of Health Technology and Informatics, Hong Kong Polytechnic University, Hong Kong, Hong Kong. [110]Manchester Royal Eye Hospital, Manchester University NHS Foundation Trust, Manchester Academic Health Science Centre, Manchester, UK. [111]School of Computer Science and Mathematics, Kingston University, Surrey, UK. [112]Section of Epidemiology and Biostatistics, Leeds Institute of Cancer and Pathology, University of Leeds, Leeds, UK. [113]Primary Care & Public Health Sciences, King's College London, London, UK. [114]Faculty of Medicine University of Southampton, Southampton General Hospital, Southampton, UK. [115]School of Medicine, Dentistry and Biomedical Sciences, Queen's University Belfast, Belfast, Northern Ireland, UK. [116]Optometry and Visual Science, School of Health Science, City, University of London, London, UK. [117]Division of Health Sciences & Centre for Clinical Brain Sciences, University of Edinburgh, Edinburgh, UK. [118]School of Clinical Sciences, Faculty of Medicine and Dentistry, University of Bristol, Bristol, UK. [119]Department of Psychiatry, Oxford University, Warneford Hospital, Oxford, UK. [120]Department of Eye and Vision Science, University of Liverpool, Liverpool, UK. [121]Centre for Experimental Medicine, Queen's University Belfast, Belfast, Northern Ireland, UK. [122]Department of Ophthalmology, University of Southampton NHS Foundation Trust, Southampton, UK. [123]Edinburgh Imaging, University of Edinburgh, Edinburgh, UK. [124]Leeds Institute of Rheumatic and Musculoskeletal Medicine, University of Leeds, Leeds, UK. [125]Department of Ophthalmology, Cambridge University Hospitals NHS Foundation Trust, Cambridge, UK. [126]Centre for Public Health, Queen's University Belfast, Belfast, Northern Ireland, UK. [127]Department of Ophthalmology, Leeds Teaching Hospitals NHS Trust, Leeds, UK. [128]Department of Ophthalmology, King's College Hospital NHS Foundation Trust, London, UK. [129]St George's, University of London, London, UK. [130]UCL Institute of Neurology, London, UK. [131]Clinical and Experimental Sciences, Faculty of Medicine, University of Southampton, Southampton, UK. [132]Institute of Genetic Medicine, Newcastle University, Newcastle Upon Tyne, UK. [133]Gloucestershire Retinal Research Group, Gloucestershire Hospitals NHS Foundation Trust, Cheltenham General Hospital, Cheltenham, UK. [134]Centre for Medical Informatics, Usher Institute for Population Health Sciences and Informatics, University of Edinburgh, Edinburgh, UK. [135]School of Science and Engineering, University of Dundee, Dundee, UK. [136]Nottingham University Hospitals NHS Trust, Nottingham, UK. [137]Norwich Medical School, University of East Anglia, Norwich, Norfolk, UK.

Methods

Ethics statement. All human research was approved by the relevant institutional review boards and/or medical ethics committees (listed in Supplementary Note) and conducted according to the Declaration of Helsinki. All CREAM participants provided written informed consent; all 23andMe applicants provided informed consent online and answered surveys according to 23andMe's human subjects protocol, which was reviewed and approved by Ethical & Independent Review Services, an AAHRPP-accredited institutional review board. The UK Biobank received ethical approval from the National Health Service National Research Ethics Service (reference 11/NW/0382).

Study data. The study populations were participants of the Consortium for Refractive Error and Myopia (CREAM) (41,793 individuals of European ancestry from 26 cohorts (CREAM-EUR) and 11,935 individuals of Asian ancestry from eight studies (CREAM-ASN)) and customers of the 23andMe genetic testing company who provided informed consent for inclusion in research studies (104,293 individuals (two cohorts of individuals with European ancestry, $n=12{,}128$ and $n=92{,}165$, respectively)). All participants included in this analysis from CREAM and 23andMe were 25 years of age or older. Participants with conditions that might alter refraction, such as cataract surgery, laser refractive procedures, retinal detachment surgery, keratoconus, or ocular or systemic syndromes were excluded from the analyses. Recruitment and ascertainment strategies varied by study (Supplementary Table 1a,b and Supplementary Note). Refractive error represented by measurements of refraction and analyzed as spherical equivalent (SphE = spherical refractive error +1/2 cylinder refractive error) was the outcome variable for CREAM; myopic refractive error was represented by self-reported AODM for 23andMe[27].

Genotype calling and imputation. Samples were genotyped on different platforms, and study-specific quality control (QC) measures of the genotyped variants were implemented before association analysis (Supplementary Table 1b). Genotypes were imputed with the appropriate ancestry-matched reference panel for all cohorts from the 1000 Genomes Project (Phase I version 3, March 2012 release) with either minimac[96] or IMPUTE[97]. The metrics for preimputation QC varied among studies, but genotype call-rate thresholds were set at a high level (≥0.95 for both CREAM and 23andMe). These metrics were similar to those of our previous GWAS analyses[26,27]; details per cohort can be found in Supplementary Table 1b.

GWAS per study. For each CREAM cohort, a single-marker analysis for the phenotype of SphE (in diopters) was carried out with linear regression with adjustment for age, sex and up to the first five principal components. For all non-family-based cohorts, one of each pair of relatives was removed (after detection through either GCTA or identity by sequence (IBS)/identity by descent (IBD) analysis). In family-based cohorts, a score test-based association was used to adjust for within-family relatedness[98]. For the 23andMe participants, Cox proportional hazards analysis testing with AODM as the dependent variable was performed as previously described[27], and P was calculated with a likelihood-ratio test for the single-marker genotype term. We used an additive SNP allelic-effect model for all analyses.

Centralized quality control per study. After individual GWAS, all studies were subjected to a second round of QC. Quantile–quantile, effect-allele frequency, P–Z test, standard error–sample size, and genomic-control inflation-factor plots were generated for each individual cohort in EasyQC[99] (Supplementary Fig. 2). All analytical issues discovered during this QC step were resolved per individual cohort.

GWAS meta-analyses. The GWAS meta-analyses were performed in three stages (Supplementary Fig. 1). In stage 1, European (CREAM-EUR, $n=44{,}192$) and Asian (CREAM-ASN, $n=11{,}935$) participants from the CREAM cohort were meta-analyzed separately. Subsequently, all CREAM cohorts (CREAM-ALL) were meta-analyzed. Variants with MAF <1% or imputation quality score <0.3 (info metric of IMPUTE) or Rsq <0.3 (minimac) were excluded. A fixed-effects inverse-variance-weighted meta-analysis was performed in METAL[100]. 1,063 variants clustering in 24 loci (Supplementary Table 2) were genome-wide significant ($P=5.0\times10^{-8}$). All 37 loci that were previously found by CREAM and 23andMe by using genotype data imputed to the HapMap II reference panel were replicated ($P_{\text{Bonferroni}}\ 1.85\times10^{-3}$), and 36 of the 37 were genome-wide significant[26,27] (Supplementary Table 2). In stage 2, a meta-analysis of the two 23andMe cohorts ($n_{23\text{andMe\_V2}}=12{,}128$; $n_{23\text{andMe\_V3}}=92{,}165$) was performed with similar filtering but a lower MAF threshold (<0.5%). A total of 5,205 genome-wide-significant variants clustered in 112 loci (Supplementary Table 2).

In stage 3, CREAM-ALL and 23andMe samples were combined through a fixed effects meta-analysis based on P value and direction of effect. In all stages, each genetic variant had to be represented by at least half of the entire study population and represented by at least 13 cohorts in CREAM and one cohort in 23andMe. For SNPs with high heterogeneity (at $P<0.05$), we also performed a random-effects meta-analysis in METASOFT[49]. We chose a different weighting scheme because of the differences in effect-size scaling. 23andMe used a less accurate phenotype variable (AODM): the effective sample size for 23andMe was approximately equivalent to the effective sample size of CREAM-ALL (Fig. 2b), and thus weighting by $(1/\sqrt{n_{\text{effective}}})$ yielded a final weighting ratio of 1:1 (ref. [101]). Genome-wide statistical significance was defined at $P<5.0\times10^{-8}$ (ref. [102]).

All three meta-analysis stages were performed under genomic control. Study-specific and meta-analysis lambda (λ) estimates are shown in Supplementary Fig. 6; to check for confounding biases (for example, cryptic relatedness and population stratification), LD-score intercepts from LD-score regressions per ancestry were constructed[30] (Supplementary Fig. 7). To check the robustness of signals, we ran conventional random-effects models in METASOFT, and fixed-effects models weighted on sample size and on weights estimated from standard error per allele were tested in METAL (Supplementary Table 2 and Supplementary Table 3).

Manhattan (modified version of package 'qqman'), regional, box and forest plots were made in R version 3.2.3 and LocusZoom[103]. An overview of the Hardy–Weinberg P of all index variants per cohort can be found in Supplementary Table 4. The comparison between refractive error and age of onset was performed in the LDSC program[30].

Population stratification and heritability calculations. Each study assessed the degree of genetic admixture and stratification in study participants through the use of principal components. Homogeneity of participants was ensured by removal of all individuals whose ancestry did not match the prevailing ancestral group. We used genomic inflation factors to control for admixture and stratification, and performed genomic-controlled meta-analysis to account for the effects of any residual heterogeneity. To further distinguish between inflation from a true polygenic signal and population stratification, we examined the relationship between test statistics and LD with LDSC. CREAM-EUR, CREAM-ASN and 23andMe were evaluated separately; variants not present in HapMap3 and with MAF <1% were excluded. SNP heritability estimates were calculated in LDSC for the same set of genetic variants.

Locus definition and annotation. All study effect-size estimates were oriented to the positive strand of the NCBI Build 37 reference sequence of the human genome. The index variant of a locus was defined as the variant with the lowest P in a region spanning a 100-kb window of the outermost genome-wide-significant variant of that same region. We annotated all index variants in the web version of ANNOVAR[104] based on UCSC Known Gene Database[34]. For variants within the coding sequence or 5′ or 3′ UTRs of a gene, that gene was assigned to the index variant (this procedure led to more than one gene being assigned to variants located within the transcription units of multiple overlapping genes). For variants in intergenic regions, the nearest 5′ gene and the nearest 3′ gene were assigned to the variant. Index variants were annotated to functional RNA elements when they were described as such in the UCSC Known Gene Database. We used conservation (PhyloP[105]) and prediction tools (SIFT[38], MutationTaster[106], align GVGD[39,40] and PolyPhen-2 (ref. [35])) to predict the pathogenicity of protein-altering exonic variants.

Conditional signal analysis. We performed conditional analysis to identify additional independent signals near the index variant at each locus, by using GCTA-COJO[32]. We transformed the Z scores of the summary statistics to betas with the following formula: standard error $=\sqrt{1/2N\times MAF(1-MAF)}$. We performed the GCTA-COJO analysis[32] by using summary-level statistics from the meta-analysis on all cohorts. LD between variants was estimated from RSI–III.

Replication in UK Biobank. The UKEV Consortium performed a GWAS of refractive error in 95,505 participants of European ancestry who were 37–73 years of age and had no history of eye disorders[33]. Refractive error was measured with an autorefractor; SphE was calculated per eye and averaged between the two eyes. To account for relatedness, a mixed-model analysis with BOLT-LMM was used[107], including age, sex, genotyping array and the first ten principal components as covariates. Analysis was restricted to markers present in the HRC reference panel[108]. We performed lookups for all independent genetic variants identified in our stage 3 meta-analysis and conditional analysis. For 16 variants not present in UKEV, we performed lookups for a surrogate variant in high LD ($r^2>0.8$). When more than one potential surrogate variant was available, the variant in strongest LD with the index variant was selected. Six variants were not available for replication: one variant (rs188159083) was neither present on the array nor was a surrogate available in UKEV, and five variants showed evidence of departure from HWE (HWE exact test $P<3.0\times10^{-4}$).

Post-GWAS analyses. We performed two gene-based tests to identify additional significant genes not found in the single-variant analysis. First, we applied the gene-based test implemented in fastBAT[41] to the per-variant summary statistics of the meta-analysis of all European cohorts (23andMe and CREAM-EUR). We used the default parameters (all variants in or within 50 kb of a gene) and focused on variants with a gene-based $P<2\times10^{-6}$ (Bonferroni correction based on 25,000 genes) and per-variant $P>5\times10^{-8}$. Second, we applied another gene-based test in EUGENE[42], which includes only variants that are eQTLs (Genotype

Tissue Expression (GTEx) data, blood[109]). EUGENE tests a hypothesis predicated on eQTLs as key drivers of the association signal. eQTLs within 50 kb of a gene were included in the test. Genes with EUGENE $P<2\times10^{-6}$ (and not found in the single variant analysis) were considered significant. Finally, we used functional annotation information from genome-wide-significant loci to reweigh results in fgwas (version 0.3.64 (ref. [43-])). Fgwas incorporates functional annotation (for example, DNase I–hypersensitive sites in various tissues and 3′-UTR regions) to reweight data from GWAS and uses a Bayesian model to calculate a posterior probability of association. This approach can identify risk loci that otherwise might not reach the genome-wide-significance threshold in standard GWAS. Details about this approach can be found in the Supplementary Note.

Refractive errors and myopia risk prediction. To assess the risk of the entire range of refractive errors, we computed PGRS values for the population-based RSI–III, using the *P* and *Z* scores from a meta-analysis on CREAM-ALL and 23andMe, excluding the RSI–III cohorts. Only variants with high imputation quality (IMPUTE info score >0.5 or minimac Rsq >0.8) and MAF >1% were considered. *P*-based clumping was performed in PLINK[110], with an r^2 threshold of 0.2 and a physical-distance threshold of 500 kb, excluding the MHC region. This procedure resulted in a total of 243,938 variants. For each individual in RSI, RSII and RSIII ($n=10{,}792$), PGRS values were calculated with the --score command in PLINK across the following strata of *P* thresholds: 5.0×10^{-8}, 5.0×10^{-7}, 5.0×10^{-6}, 5.0×10^{-5}, 5.0×10^{-4}, 0.005, 0.01, 0.05, 0.1, 0.5, 0.8 and 1.0. The proportion of variance explained by each PGRS model was calculated as the difference in the R^2 between two regression models: one in which SphE was regressed on age, sex and the first five principal components, and the other also including the PGRS as an additional covariate. Subsequently, areas under the receiver operating characteristic curve were calculated for myopia (SphE ≤−3 s.d.) vs. hyperopia (SphE ≥+3 s.d.).

Genetic correlation between ancestries. We used Popcorn[47] to investigate ancestry-related differences in the genetic architecture of refractive error and myopia. Popcorn takes summary GWAS statistics from two populations and LD information from ancestry-matched reference panels, and computes genetic correlations by implementing a weighted likelihood function that accounts for the inflation of *Z* scores due to LD. Pairwise analyses were carried out by using the GWAS summary statistics from 23andMe ($n=104{,}292$), CREAM-EUR ($n=44{,}192$) and CREAM-EAS ($n=9{,}826$) meta-analyses. Only SNPs with MAF ≥5% were included, thus resulting in a final set of 3,625,602 SNPs for analyses involving 23andMe and 3,642,928 SNPs for the CREAM-EUR vs. CREAM-EAS analysis. Reference panels were constructed with genotype data from 503 European and 504 East Asian individuals sequenced as part of the 1000 Genomes Project (release 2 May 2013; see URLs). The reference-panel VCF files were filtered in PLINK[110] to remove indels, strand-ambiguous variants, variants without an 'rs' ID prefix and variants located in the MHC region on chromosome 6 (chromosome 6: 25000000–33500000; build 37).

Analysis between phenotypes. To evaluate the consistency of genotypic effects across studies that used different phenotype definitions, we compared effect sizes from GWAS studies of either SphE or AODM in Europeans, i.e., CREAM-EUR ($n=44{,}192$) or 23andMe ($n=104{,}293$), respectively. Marker-wise additive genetic effect sizes (in diopters per copy of the risk allele) for SphE were compared against those (in units log(HR) per copy of the risk allele) for AODM. Data were visualized with R. Genetic correlation between the two phenotypes SphE and AODM was calculated through LD-score regression. This analysis included all common SNPs (MAF >0.01) present in HapMap3.

Evidence of functional involvement. To rank genes according to biological plausibility, we scored annotated genes according to our own findings and published reports of a potential functional role in refractive error. Points were assigned for each gene on the basis of ten categories (details on the methodology per category are provided in Supplementary Note): internal replication of index genetic variants in the individual cohort GWAS analyses through Bonferroni correction (CREAM-ASN, CREAM-EUR and 23andMe; $P_{\text{Bonferroni}}$ 1.19×10^{-4}); evidence of eQTL from FUMA[32] analysis and extensive lookups in GTEx; evidence of expression in the eye in developmental ocular tissues; evidence of expression in the eye in adult ocular tissues; presence of an eye phenotype in knockout mice (Mouse Genome Informatics and International Mouse Phenotyping Consortium databases); presence of an eye phenotype in humans (OMIM; see URLs, DisGeNET[111]); location in a functional region of a gene (wANNOVAR; see URLs); presence of the gene in a significant enriched functional pathway with FDR <0.05 (DEPICT[48]); presence of the gene in the gene priority analysis of DEPICT with FDR <0.05; and presence of the gene in the canonical pathway analysis of IPA (see URLs). Furthermore, we performed a systematic search for each gene to assess its potential as a drug target (SuperTarget[112], STITCH[113], DrugBank[114] and PharmaGkb[115]). All information derived from this study and the literature was used to annotate genes to retinal cell types.

Genetic pleiotropy. To investigate the overlap of genes with other common traits, we performed a lookup in the GWAS catalog by using FUMA. Multiple-testing correction (i.e., Benjamini–Hochberg) was performed. Traits were significantly associated when adjusted $P\leq0.05$, and the number of genes that overlapped with the GWAS-catalog gene sets was ≥2.

Reporting Summary. Further information on experimental design is available in the Nature Research Reporting Summary linked to this article.

Data availability. The summary statistics of the stage 3 meta-analysis are included in Supplementary Data 3. To protect the privacy of the participants in our cohorts, further summary statistics of stage 1 (CREAM) and stage 2 (23andMe) will be available upon reasonable request. Please contact c.c.w.klaver@erasmusmc.nl (CREAM) and/or apply.research@23andMe.com (23andMe) for more information and to access the data.

References

96. Howie, B., Fuchsberger, C., Stephens, M., Marchini, J. & Abecasis, G. R. Fast and accurate genotype imputation in genome-wide association studies through pre-phasing. *Nat. Genet.* **44**, 955–959 (2012).
97. Marchini, J., Howie, B., Myers, S., McVean, G. & Donnelly, P. A new multipoint method for genome-wide association studies by imputation of genotypes. *Nat. Genet.* **39**, 906–913 (2007).
98. Chen, W. M. & Abecasis, G. R. Family-based association tests for genomewide association scans. *Am. J. Hum. Genet.* **81**, 913–926 (2007).
99. Winkler, T. W. et al. Quality control and conduct of genome-wide association meta-analyses. *Nat. Protoc.* **9**, 1192–1212 (2014).
100. Willer, C. J., Li, Y. & Abecasis, G. R. METAL: fast and efficient meta-analysis of genomewide association scans. *Bioinformatics* **26**, 2190–2191 (2010).
101. Zaykin, D. V. Optimally weighted Z-test is a powerful method for combining probabilities in meta-analysis. *J. Evol. Biol.* **24**, 1836–1841 (2011).
102. Dudbridge, F. & Gusnanto, A. Estimation of significance thresholds for genomewide association scans. *Genet. Epidemiol.* **32**, 227–234 (2008).
103. Pruim, R. J. et al. LocusZoom: regional visualization of genome-wide association scan results. *Bioinformatics* **26**, 2336–2337 (2010).
104. Yang, H. & Wang, K. Genomic variant annotation and prioritization with ANNOVAR and wANNOVAR. *Nat. Protoc.* **10**, 1556–1566 (2015).
105. Cooper, G. M. et al. Distribution and intensity of constraint in mammalian genomic sequence. *Genome Res.* **15**, 901–913 (2005).
106. Schwarz, J. M., Rödelsperger, C., Schuelke, M. & Seelow, D. MutationTaster evaluates disease-causing potential of sequence alterations. *Nat. Methods* **7**, 575–576 (2010).
107. Loh, P. R. et al. Efficient Bayesian mixed-model analysis increases association power in large cohorts. *Nat. Genet.* **47**, 284–290 (2015).
108. McCarthy, S. et al. A reference panel of 64,976 haplotypes for genotype imputation. *Nat. Genet.* **48**, 1279–1283 (2016).
109. Consortium, G. T., GTEx Consortium. The Genotype-Tissue Expression (GTEx) pilot analysis: multitissue gene regulation in humans. *Science* **348**, 648–660 (2015).
110. Chang, C. C. et al. Second-generation PLINK: rising to the challenge of larger and richer datasets. *Gigascience* **4**, 7 (2015).
111. Bauer-Mehren, A., Rautschka, M., Sanz, F. & Furlong, L. I. DisGeNET: a Cytoscape plugin to visualize, integrate, search and analyze gene-disease networks. *Bioinformatics* **26**, 2924–2926 (2010).
112. Günther, S. et al. SuperTarget and Matador: resources for exploring drug-target relationships. *Nucleic Acids Res.* **36**, D919–D922 (2008).
113. Kuhn, M. et al. STITCH 4: integration of protein-chemical interactions with user data. *Nucleic Acids Res.* **42**, D401–D407 (2014).
114. Wishart, D. S. et al. DrugBank: a comprehensive resource for in silico drug discovery and exploration. *Nucleic Acids Res.* **34**, D668–D672 (2006).
115. Whirl-Carrillo, M. et al. Pharmacogenomics knowledge for personalized medicine. *Clin. Pharmacol. Ther.* **92**, 414–417 (2012).

Corresponding Author: CCW Klaver

Date: Feb 26, 2018

Life Sciences Reporting Summary

Nature Research wishes to improve the reproducibility of the work we publish. This form is published with all life science papers and is intended to promote consistency and transparency in reporting. All life sciences submissions use this form; while some list items might not apply to an individual manuscript, all fields must be completed for clarity.

For further information on the points included in this form, see Reporting Life Sciences Research. For further information on Nature Research policies, including our data availability policy, see Authors & Referees and the Editorial Policy Checklist.

Experimental design

1. Sample size

   Describe how sample size was determined.

   Our strategy aimed to create the largest possible sample size for the meta-analysis and we initially included practically all existing population studies with genetic and refractive error data in our analysis. Furthermore, for the replication analysis, we used the summary statistics of the GWAS from the UKEV consortium based on refractive error. We performed a power calculation using G*Power 3.1.9.2 in order to check the power of the sample size of this cohort (n= 95,505): the two-sided linear multiple regression t-test with a mean effect of 0.03, an alfa of 0.000299 (0.05/167) and at least 80% power, the appropriate sample size for replication should comprise at least 669 participants. The UKEV cohort is the largest and only other independent cohort known in the world with this similar accurate phenotype.

2. Data exclusions

   Describe any data exclusions.

   Every cohort removed participants with conditions that could alter refraction, such as cataract surgery, laser refractive procedures, retinal detachment surgery, keratoconus as well as ocular or systemic syndromes.

3. Replication

   Describe whether the experimental findings were reliably reproduced.

   There are no other existing large studies to replicate our findings to date. We performed internal and independent replications.
   We found significant overlap in the internal replications: all 25 loci identified at Stage 1 (CREAM) replicated in Stage 2 (23andMe; pBonferroni 2.00 x 10-3). Vice versa, 29 (25.9%) of the loci identified at Stage 2 replicated in Stage 1 (pBonferroni 4.46 x 10-4), an expected proportion given the lower statistical power in CREAM.
   Furthermore, we replicated in an independent cohort consisting of 95,505 participants. In the GWAS on refractive error performed by the UK Biobank Eye & Vision Consortium, we replicated 86% of all independent loci.

4. Randomization

   Describe how samples/organisms/participants were allocated into experimental groups.

   Randomization was not relevant to our GWAS meta-analysis study; we performed an overall meta-analyses of all available data.

5. Blinding

   Describe whether the investigators were blinded to group allocation during data collection and/or analysis.

   Blinding was not relevant to our study; our analysts only had access to summary statistics of GWAS analyses.

Note: all studies involving animals and/or human research participants must disclose whether blinding and randomization were used.

6. Statistical parameters

For all figures and tables that use statistical methods, confirm that the following items are present in relevant figure legends (or the Methods section if additional space is needed).

n/a	Confirmed	
☐	☒	The exact sample size (*n*) for each experimental group/condition, given as a discrete number and unit of measurement (animals, litters, cultures, etc.)
☐	☒	A description of how samples were collected, noting whether measurements were taken from distinct samples or whether the same sample was measured repeatedly.
☒	☐	A statement indicating how many times each experiment was replicated
☐	☒	The statistical test(s) used and whether they are one- or two-sided (note: only common tests should be described solely by name; more complex techniques should be described in the Methods section)
☐	☒	A description of any assumptions or corrections, such as an adjustment for multiple comparisons
☐	☒	The test results (e.g. *p* values) given as exact values whenever possible and with confidence intervals noted
☐	☒	A summary of the descriptive statistics, including central tendency (e.g. median, mean) and variation (e.g. standard deviation, interquartile range)
☐	☒	Clearly defined error bars

See the web collection on statistics for biologists for further resources and guidance.

Software

Policy information about availability of computer code

7. Software

Describe the software used to analyze the data in this study.

R version 3.2.3 (packages: qqman, ggplot2, metafor); Minimac, IMPUTE (imputations); EasyQC version: 9.0 (quality control); METAL 2011-03-25 release (GWAS meta-analyses); LocusZoom (regional plots); LDSC https://github.com/bulik/ldsc (LD score regression); GCTA64 version 1.26.0 (conditional analyses); fastbat, EUGENE, fgwas (post GWAS analyses); PLINK v1.9 (clumping for PGRS); Popcorn https://github.com/brielin/Popcorn (ancestry-related differences); FUMA (eQTLS & GWAS catalogue look up); DEPICT v1 release 194, Cytoscape version 3.4.0, IPA (pathway analysis); Polyphen (http://genetics.bwh.harvard.edu/pph2/); SIFT (http://sift.jcvi.org/www/SIFT_aligned_seqs_submit.html); Mutation Taster (http://www.mutationtaster.org/); METASOFT v2.0.1 (Random Effects meta-analyses)

For all studies, we encourage code deposition in a community repository (e.g. GitHub). Authors must make computer code available to editors and reviewers upon request. The *Nature Methods* guidance for providing algorithms and software for publication may be useful for any submission.

Materials and reagents

Policy information about availability of materials

8. Materials availability

Indicate whether there are restrictions on availability of unique materials or if these materials are only available for distribution by a for-profit company.

No unique materials were used.

9. Antibodies

Describe the antibodies used and how they were validated for use in the system under study (i.e. assay and species).

No antibodies were used.

10. Eukaryotic cell lines

a. State the source of each eukaryotic cell line used.

No eukaryotic cell lines were used.

b. Describe the method of cell line authentication used.

No eukaryotic cell lines were used.

c. Report whether the cell lines were tested for mycoplasma contamination.

No eukaryotic cell lines were used.

d. If any of the cell lines used in the paper are listed in the database of commonly misidentified cell lines maintained by ICLAC, provide a scientific rationale for their use.

No commonly misidentified cell lines were used.

Animals and human research participants

Policy information about studies involving animals; when reporting animal research, follow the ARRIVE guidelines

11. Description of research animals

Provide details on animals and/or animal-derived materials used in the study.

No animals were used.

Policy information about studies involving human research participants

12. Description of human research participants

Describe the covariate-relevant population characteristics of the human research participants.

All participants included in this analysis from CREAM and 23andMe were aged 25 years or older. Participants with conditions that could alter refraction, such as cataract surgery, laser refractive procedures, retinal detachment surgery, keratoconus as well as ocular or systemic syndromes were excluded from the analyses. All relevant information on the study participants, including mean age, gender, and refractive error is stated in Supplementary Table 1a,b. No individual genotype data are shared. Refractive error represented by measurements of refraction and analyzed as spherical equivalent (SphE =spherical refractive error + 1/2 cylinder refractive error) was the outcome variable for CREAM; myopic refractive error represented by self-reported age of diagnosis of myopia (AODM) for 23andMe. For each CREAM cohort, a single marker analysis for the SphE (in diopters) phenotype was carried out using linear regression adjusting for age, sex and up to the first five principal components.